

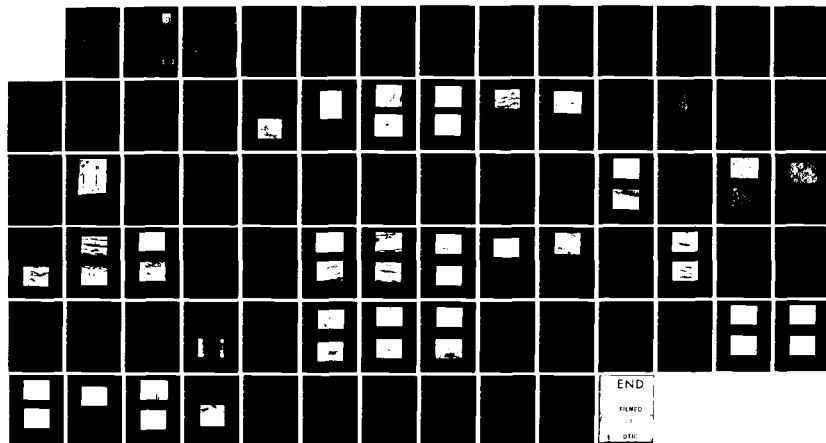
AD-A123 254

RESEARCH ON TRANSVERSE REINFORCEMENT OF BOND LINES VIA
IN SITU FIBERIZATION. (U) HUGHES AIRCRAFT CO EL SEGUNDO
CA ELECTRO-OPTICAL AND DATA SYS. C H SHERWOOD ET AL.
OCT 82 HAC-FR-82-76-900 AFWAL-TR-82-4119 F/G 11/5

1/1

UNCLASSIFIED

NL





Number of hauls	<i>P. setiferus</i> (%)	<i>P. setiferus</i> + <i>P. setiferus</i> + <i>P. setiferus</i> (%)
1	100	0
2	80	20
3	60	40
4	40	60
5	20	80
6	10	90
7	10	90
8	10	90
9	10	90
10	10	90

12

HAC REPORT NO. FR-82-76-900
HAC REF. NO. E8699

AFWAL-TR-82-4119

RESEARCH ON TRANSVERSE REINFORCEMENT OF
BOND LINES VIA IN SITU FIBERIZATION



C. H. SHERWOOD
P. J. SHERMAN

HUGHES AIRCRAFT COMPANY
TECHNOLOGY SUPPORT DIVISION
ELECTRO OPTICAL AND DATA SYSTEMS GROUP
CULVER CITY, CALIFORNIA 90230

OCTOBER 1982

Report for Period:
26 MARCH 1981 TO 15 JULY 1982

APPROVED FOR PUBLIC RELEASE; DISTRIBUTION UNLIMITED

DTIC
ELECTE
JAN 11 1983
B

MATERIALS LABORATORY
AIR FORCE WRIGHT AERONAUTICAL LABORATORIES
AIR FORCE SYSTEMS COMMAND
WRIGHT-PATTERSON AIR FORCE BASE, OHIO 45433

73 01 11 010

AD A 123254


DTIC FILE COPY

NOTICE

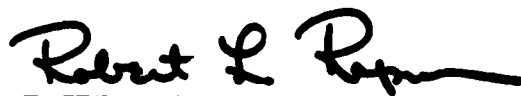
When Government drawings, specifications, or other data are used for any purpose other than in connection with a definitely related Government procurement operation, the United States Government thereby incurs no responsibility nor any obligation whatsoever; and the fact that the government may have formulated, furnished, or in any way supplied the said drawings, specifications, or other data, is not to be regarded by implication or otherwise as in any manner licensing the holder or any other person or corporation, or conveying any rights or permission to manufacture, use, or sell any patented invention that may in any way be related thereto.

This report has been reviewed by the Office of Public Affairs (ASD/PA) and is releasable to the National Technical Information Service (NTIS). At NTIS, it will be available to the general public, including foreign nationals.

This technical report has been reviewed and is approved for publication.



HERBERT S. SCHWARTZ, Matls Rech Engr
Composites, Adhesives & Fibrous Matls Br



ROBERT L. RAPSON, Acting Chief
Composites, Adhesives & Fibrous Matls Br

FOR THE COMMANDER:



FRANKLIN D. CHERRY, Chief
Nonmetallic Materials Division

"If your address has changed, if you wish to be removed from our mailing list, or if the addressee is no longer employed by your organization please notify AFWAL/MLBC, W-P AFB, OH 45433 to help maintain a current mailing list".

Copies of this report should not be returned unless return is required by security considerations, contractual obligations, or notice on a specific document.

UNCLASSIFIED

SECURITY CLASSIFICATION OF THIS PAGE (When Data Entered)

REPORT DOCUMENTATION PAGE		READ INSTRUCTIONS BEFORE COMPLETING FORM
1. REPORT NUMBER AFWAL-TR-82-4119	2. GOVT ACCESSION NO. AD-A223254	3. RECIPIENT'S CATALOG NUMBER
4. TITLE (and Subtitle) RESEARCH ON TRANSVERSE REINFORCEMENT OF BOND LINES VIA IN SITU FIBERIZATION		5. TYPE OF REPORT & PERIOD COVERED Final Report - March 1981 to July 1982
		6. PERFORMING ORG. REPORT NUMBER FR-82-76-900
7. AUTHOR(s) C. H. Sherwood P. J. Sherman		8. CONTRACT OR GRANT NUMBER(s) F33615-81-C-5009
9. PERFORMING ORGANIZATION NAME AND ADDRESS Hughes Aircraft Company, Electro-Optical & Data Systems Group, Culver City, California 90230		10. PROGRAM ELEMENT, PROJECT, TASK AREA & WORK UNIT NUMBERS
11. CONTROLLING OFFICE NAME AND ADDRESS Air Force Wright Aeronautical Laboratories (AFWAL/ MLBC), Air Force Systems Command, Wright- Patterson AFB, Ohio 45433		12. REPORT DATE October 1982
		13. NUMBER OF PAGES 77
14. MONITORING AGENCY NAME & ADDRESS (If different from Controlling Office)		15. SECURITY CLASS. (of this report) UNCLASSIFIED
		15a. DECLASSIFICATION/DOWNGRADING SCHEDULE
16. DISTRIBUTION STATEMENT (of this Report) Approved for public release; distribution unlimited		
17. DISTRIBUTION STATEMENT (of the abstract entered in Block 20, if different from Report)		
18. SUPPLEMENTARY NOTES		
19. KEY WORDS (Continue on reverse side if necessary and identify by block number) In situ formed polymeric fibers, flow induced crystallization, fiber reinforced adhesives, shish kebab morphology.		
20. ABSTRACT (Continue on reverse side if necessary and identify by block number) The intent of the program was to investigate the utility of in situ formed poly- propylene fibers as a reinforcement to increase the peel and cleavage perfor- mance of adhesively bonded joints. Specifically, phosphoric acid anodized aluminum substrates were used with the aim of producing fibers via flow induced crystallization directly in the pore structure which would extend out into and reinforce the adhesive resin. Experimental results have shown that the in situ formed polypropylene fibers do have dimensions compatible with the pore sizes of		

DD FORM 1473

1 JAN 73

EDITION OF 1 NOV 65 IS OBSOLETE

UNCLASSIFIED

SECURITY CLASSIFICATION OF THIS PAGE (When Data Entered)

UNCLASSIFIED

SECURITY CLASSIFICATION OF THIS PAGE(When Data Entered)

the anodic layers produced and there is some evidence to suggest that formation does take place within the pores. Further, it was demonstrated that adhesion to the polypropylene material could be enhanced by plasma treatments; in particular, short time, medium power, oxygen exposures. Bonded T-peel and lap shear specimens were tested and the most promising results for fiberized specimens were in general equal to those obtained with non-fiberized control samples. Subsequent failure analysis revealed that problems of adhesive penetration and fiber film formation were responsible, at least in part, for the reduced mechanical performance. In conclusion, this program has explored a truly interesting concept which may indeed have potential. The results obtained have served to show feasibility but considerably more developmental effort is required to demonstrate reduction to practicality.

UNCLASSIFIED

SECURITY CLASSIFICATION OF THIS PAGE(When Data Entered)

FOREWORD

This final report on the program "Research on Transverse Reinforcement of Bond Lines via In Situ Fiberization" presents the results of work performed during the period 26 March 1981 through 15 July 1982 under Contract F33615-81-C-5009 with the United States Air Force, Air Force Systems Command, Air Force Wright Aeronautical Laboratories (AFWAL/MLBC), Wright-Patterson Air Force Base, Ohio. The work, monitored by Mr. Herbert S. Schwartz, was undertaken within the Technology Development Laboratory of the Technology Support Division of the Electro-Optical and Data System Group of the Hughes Aircraft Company. The Program Manager and Principal Investigator was Dr. C. H. Sherwood.

The efforts of several people from the Technology Support Division who made significant contributions to this program must be acknowledged. This includes Mr. G. L. Meldrum and Mr. R. R. Muego for providing SEM and mechanical property data, respectively. Special thanks must go to Mr. F. J. Ricaud, who conducted the aluminum surface treatment portion of this program.



Accession For	
NTIS GRA&I	<input checked="checked" type="checkbox"/>
DTIC TAB	<input type="checkbox"/>
Unannounced	<input type="checkbox"/>
Justification	
By	
Distribution/	
Availability Codes	
Dist	Avail and/or Special
A	

TABLE OF CONTENTS

SECTION		
I	INTRODUCTION	1
	1. Program Objective	1
	2. Flow Induced Crystallization	2
	3. Hughes In Situ Fiber (ISF) Technology Development	5
	4. Fundamental Mechanism of Fiber Formation from Solution	10
II	EXPERIMENTAL	14
	1. Material	14
	2. Equipment and Procedures	15
III	RESULTS AND DISCUSSION	19
	1. Aluminum Surface Treatments	19
	2. Fiberization Optimization	32
	3. Fiber Surface Treatments	41
	4. Property Determination and Analysis	51
IV	CONCLUSIONS AND RECOMMENDATIONS	62
V	REFERENCES	64

LIST OF ILLUSTRATIONS

FIGURE		PAGE
1	Shisk Kebab Morphology	3
2	Secondary Flow Depiction in Couette Apparatus. Dashed Lines Represent Streamlines of Taylor Vortices	4
3	SEM Photograph of ISF Solution Agitation Material Which Has Been Subsequently Chopped	5
4	Regularly Spaced Tines Fiberized Via ISF. Magnification - 5X	6
5	SEM Photograph of ISF Polyethylene Fibers. Magnification - 100,000X	7
6	X-Ray Diffraction Pattern Formed by ISF Polyethylene Material	7
7	SEM Photograph of ISF Polypropylene Material. Magnification - 16,400X	8
8	SEM Photograph of ISF Poly-1-Butene Material. Magnification - 18,000X	8
9	SEM Photograph of ISF Poly-4-Methyl-1-Pentene Material. Magnification - 9,500X	9
10	Electronic Component Before and After Fiberization	10
11	Entangled Fibers Crystallized into an Oriented State via Shear Field Influence	12
12	GPC Trace for Isotactic Polypropylene	14
13	Apparatus Used for ISF Experiments	16
14	Schematic Drawing of Plasma Treatment Equipment	18
15	Oxide Thickness Versus Anodizing Voltage for Bare 7075-T6 Anodized in Phosphoric Acid	21
16	Oxide Thickness on Bare 7075-T6 versus Concentration of Phosphoric Acid Anodizing Bath	22
17	Oxide Thickness versus Anodizing Time for Bare 7075-T6 Anodized in Phosphoric Acid	22
18	Anodic Coating on 2024-T3 Clad Sample. Magnification - 24,000X	25

LIST OF ILLUSTRATIONS (Continued)

FIGURE		PAGE
19	Anodic Coating on 2024-T3 Clad Sample. Magnification - 24,000X	25
20	TEM Photomicrograph of Anodized 2024-T3 Clad Surface. Magnification - 80,000X	27
21	TEM Photomicrograph of Anodized 2024-T3 Bare Surface. Magnification - 80,000X	27
22	TEM Photomicrograph of Anodized 7075-T6 Bare Surface. Magnification - 80,000X	28
23	SEM of Anodized, Liquid Honed 2024-T3 Clad Surface. Magnification - 6,000X	29
24	SEM of Anodized 2024-T3 Clad Surface. Magnification - 6,000X	30
25	SEM of Etched 2024-T3 Clad Surface. Magnification - 6,400X	30
26	SEM of Etched 2024-T3 Clad Surface. Magnification - 14,000X	31
27	SEM of Etched 7075-T6 Bare Surface. Magnification - 24,000X	31
28	SEM Micrograph of Fiberized, Anodized 2024-T3 Clad Surface. Magnification - 6,500X	34
29	SEM Micrograph of Fiberized, Anodized 7075-T6 Bare Surface. Magnification - 6,500X	34
30	SEM Micrograph of Fiberized, Anodized 2024-T3 Bare Surface. Magnification - 6,400X	35
31	SEM Micrograph of Anodized 2024-T3 Clad Surface. Magnification - 6,000X	35
32	SEM Micrograph of Anodized 7075-T6 Bare Surface. Magnification - 6,500X	36
33	SEM Micrograph of Anodized 2024-T3 Bare Surface. Magnification - 6,000X	36
34	SEM of Fiberized Anodic Surface Showing Film Formation. Magnification - 6,400X	37
35	SEM Micrograph of Fiberized, Anodized 2024-T3 Clad Surface Subjected to Multiple Fiberizations. Magnification - 5,000X	38

LIST OF ILLUSTRATIONS (Continued)

FIGURE		PAGE
36	SEM Micrograph of Lightly Fiberized, Anodized 2024-T3 Clad Surface. Magnification - 5,000X	40
37	SEM Micrograph of Heavily Fiberized, Anodized 2024-T3 Clad Surface. Magnification - 5,700X	40
38	Sandwich Test Specimen Used with Polypropylene Film Plasma Studies	46
39	SEM Micrograph of Untreated Polypropylene Film Surface. Magnification - 5,000X	46
40	SEM Micrograph of Polypropylene Film Subjected to Extreme Oxygen Plasma Treatment. Magnification - 5,000X	48
41	SEM Micrograph of Polypropylene Film Subjected to Mild Oxygen Plasma Treatment. Magnification - 5,000X	48
42	SEM Micrograph of Polypropylene Film Treated with Helium Plasma. Magnification - 5,000X	49
43	SEM Micrograph of Polypropylene Film Treated with Acetylene Plasma. Magnification - 5,000X	49
44	SEM Micrograph of Fiberized Specimen Subjected to Long Term Helium Plasma Treatment. Magnification - 4,500X	50
45	SEM Micrograph of Fiberized Specimen Subjected to Short Term Oxygen Plasma Treatment. Magnification - 5,200X	50
46	SEM Micrograph of Lightly Fiberized Unbonded Specimen. Magnification - 10,000X	55
47	SEM Micrograph of a Fracture Surface of a Heavily Fiberized Coupon Bonded with Epon 828. Magnification - 9,000X	55
48	SEM Micrograph of Adhesive Layer Fracture Speciman. Magnification - 5,000X	56
49	SEM of Epon 828 Control Fracture Surface. Magnification - 14,000X	56
50	SEM Micrograph of Aluminum Coupon Fracture Surface of Lightly Fiberized Specimen. Magnification - 8,200X	57
51	SEM Micrograph of Adhesive Film Fracture Surface of Lightly Fiberized Specimen. Magnification - 8,200X	57

LIST OF ILLUSTRATIONS (Continued)

FIGURE		PAGE
52	SEM Micrograph of Fiberized Specimen Bonded with FM-73. Magnification - 2,200X	58
53	SEM Micrograph of Fiberized Specimen Bonded with FM-73. Magnification - 1,600X	59
54	SEM Micrograph of Sample Shown Above at 16,000X Magnification	59
55	SEM Micrograph of FM-73 Adhesive. Magnification - 2,000X	60

LIST OF TABLES

TABLE		PAGE
1	Procedure for FPL Etch	19
2	Procedure for Phosphoric Acid Anodizing	20
3	Effect of Process Temperature and Bath Concentration on Anodic Layer Thickness	24
4	Anodized Layer Thickness as a Function of Voltage	26
5	Optimum Phosphoric Acid Anodizing Conditions	28
6	Experimental Variable Investigation	
7	Shear Strength versus Treatment Conditions for Samples Bonded with Epon 828 Adhesive System	
8	Shear Strength versus Treatment Conditions for Samples Bonded with FM-73 Adhesive System	
9	Shear Strength and Peel Strength for Lightly Fiberized Coupons Bonded with FM-73 Adhesive System	52
10	Shear Strength and Peel Strength for Heavily Fiberized Coupons Bonded with FM-73 Adhesive System	52
11	Shear Strength and Peel Strength for Fiberized Coupons Bonded with Epon 828 Adhesive System	53

SUMMARY

The intent of the program was to investigate the utility of in situ formed polypropylene fibers as a reinforcement to increase the peel and cleavage performance of adhesively bonded joints. Specifically, phosphoric acid anodized aluminum substrates were used with the aim of producing fibers via flow induced crystallization directly in the pore structure which would extend out into and reinforce the adhesive resin. Experimental results have shown that the in situ formed polypropylene fibers do have dimensions compatible with the pore sizes of the anodic layers produced and there is some evidence to suggest that formation does take place within the pores. Further, it was demonstrated that adhesion to the polypropylene material could be enhanced by plasma treatments; in particular, short time, medium power, oxygen exposures. Bonded T-peel and lap shear specimens were tested and the most promising results for fiberized specimens were in general equal to those obtained with non-fiberized control samples. Subsequent failure analysis revealed that problems of adhesive penetration and fiber film formation were responsible, at least in part, for the reduced mechanical performance. In conclusion, this program has explored a truly interesting concept which may indeed have potential. The results obtained have served to show feasibility but considerably more developmental effort is required to demonstrate reduction to practicality.

SECTION I INTRODUCTION

1. Program Objective

The use of adhesives to bond primary fuselage structural members in lieu of riveting has been investigated over the last several years in the PABST (Primary Adhesively Bonded Structure Technology) and related programs^{1,2}. The findings have shown that with appropriate bonding surface design, adhesive and primer selection, and pretreatment of the metallic surfaces to be bonded, adhesives are generally capable of withstanding the necessary static and cyclic loadings which could be encountered by aircraft structures in flight. Under optimum processing conditions, the bonded part failures were observed to be cohesive rather than adhesive, indicating that the next step in improving the durability of bonded structures is to increase the strength of the bulk adhesive and its resistance to catastrophic failure by crack propagation without adversely affecting its ability to adhere to the substrate. The objective of this program was to investigate a potential technical advance in this area via the use of in situ formed fiber reinforcement of adhesive candidates. Specifically, the concept involved the precipitation of polymeric fibers from solution via flow induced crystallization. These fibers, deposited in the pores of the optimally treated metallic surfaces, would serve to strengthen the adhesive and at the same time provide a physical attachment between the bulk adhesive and the pretreated metallic substrate.

A large portion of the PABST effort was directed toward the development of specific aluminum surface structures by different chemical treatments such as phosphoric acid anodizing, chromic acid anodizing and sulphuric acid-sodium dichromate (FPL) etch. Surface character was found to vary with different treatments but a typical phosphoric acid anodizing process produced columnar oxide layers approximately 4000Å thick with a pore size on the order of 300Å. It was thought likely that by manipulation of the anodizing process parameters such as temperature, voltage, time, and acid bath concentration, this size

could be increased. Data taken from the literature³ indicated that typical polyolefin fibrils grow to diameters of 180\AA - 350\AA and lengths of several thousand angstroms depending on experimental conditions. This qualitatively agreed with observations made during ISF research at Hughes, although the emphasis in previous work was not on controlling fiber diameter. It was also important to consider the molecular coil dimensions of the polymer in solution because if these dimensions greatly exceeded that of the pore size, it would be difficult to induce crystal nucleation and growth in the pores themselves. Reported data⁴ indicated that the radius of gyration for polypropylene with a molecular weight of 10^5 was approximately 500\AA . It can be assumed that the polymer coil dimensions can be altered somewhat by the flow regime and the solvent system used and that the proposed concept was sound based on first principals. Since the majority of the program centers around the formation of in situ fibers, the remainder of this introductory section will be devoted to a discussion of the phenomenon of flow induced crystallization.

2. Flow Induced Crystallization

Flow induced crystallization of polymers from solution is now a well known phenomenon and has been extensively studied over the past fifteen years^{5,6}. The pioneering work done in this area was conducted by Pennings and coworkers⁷ who were originally attempting to fractionate different molecular weight species of polyethylene from solutions subjected to flow by vigorous stirring. The result was an interesting fibrous formation, produced at extremely high rotational speeds, which came to be known as the shish kebab morphology and is depicted in Figure 1. Exhaustive research was conducted with electron microscopy techniques to characterize the crystal structure, orientation and dimensions of these fibers as a function of formation conditions. Several predominant features of the morphology have been well established. First, the shish kebab crystals remain intact even after extensive solvent washing above the formation temperature indicating the kebabs are not simple epitaxial overgrowths but are molecularly incorporated into the fiber backbone^{8,9}. Second,

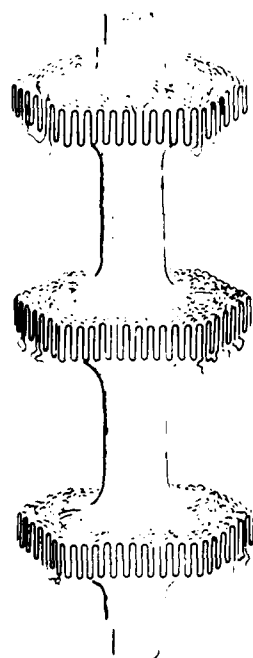


Figure 1. Shish Kebab Morphology.

epitaxial overgrowths can form over this underlying structure under certain processing conditions¹⁰. Third, geometric relationships have been observed between kebab diameter and spacing which appear to be independent of the specific flow field conditions used to produce them¹¹. Additional study of the morphology has revealed the fibrous crystals to have a very high degree of preferred orientation along the fiber axis¹² as well as intriguing melting behavior¹³ and enhanced mechanical properties¹⁴.

In addition to the study of the structure of these unique materials, considerable effort has been expended to define the flow conditions necessary to produce them. Again, Pennings and coworkers¹⁵ conducted the initial experimental work which demonstrated that elongational flow was necessary to sufficiently deform and orient aggregates of molecules in order to form primary bundle-like nuclei which subsequently grow into fibrillar crystals. This was accomplished in a Couette apparatus by inducing secondary flows, termed Taylor vortices, as shown in Figure 2. Simple shear flows, and consequently the absence of extensional velocity gradients, were ineffective in nucleating fiber formation. This work was followed by numerous studies aimed at investigating elongational flows and reproducing Pennings' findings. In particular, Frank, Mackley and Keller^{16,17} explored the use of impinging jets, Torza adapted a four roll mill¹⁸ and McHugh and coworkers¹⁹ employed an oscillating bob apparatus. It was also during this era that initial

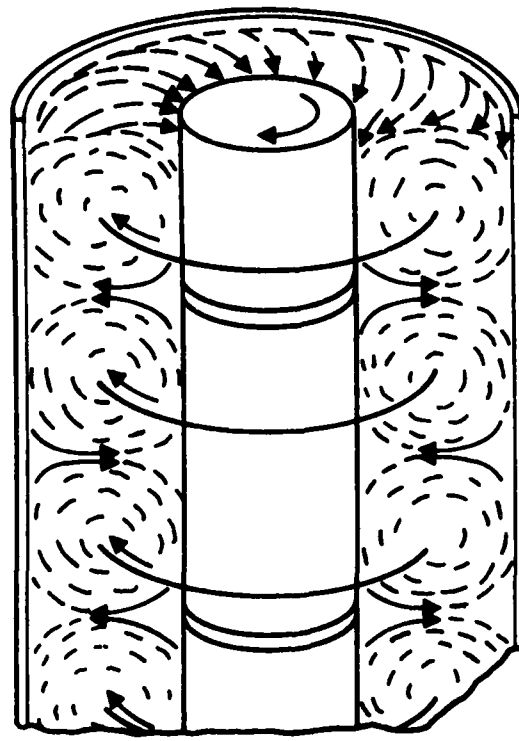


Figure 2. Secondary Flow Depiction in Couette Apparatus. Dashed Lines Represent Streamlines of Taylor Vortices.

experiments were being conducted at Hughes with the in situ fiber technology^{20,21}. It is useful at this juncture to review the development of this work.

3. Hughes In Situ Fiber (ISF) Technology Development

The initial discovery which led to the development of the ISF technology was that under conditions of low amplitude solution agitation, polymers could be induced to crystallize into what appeared to be three dimensional, interconnected networks. The first variation of this process involved the agitation of bulk dilute solutions of polymers and their containers. Using this technique, the material formed duplicated the shape of the container and filled the volume originally occupied by the solution. The structure of the material was not classical shish kebab, but was clearly fibrous as shown in Figure 3. This development was followed by a modification of the technique in which an object was oscillated in a crystallizing polymer solution. The initial experiments were conducted with simple wire configurations²² and it was found that fibers could be induced to form on these objects as shown in Figure 4. In addition, the morphology of the fibers produced was indicative of the highly oriented shish kebab material. This is clearly shown for polyethylene ISF

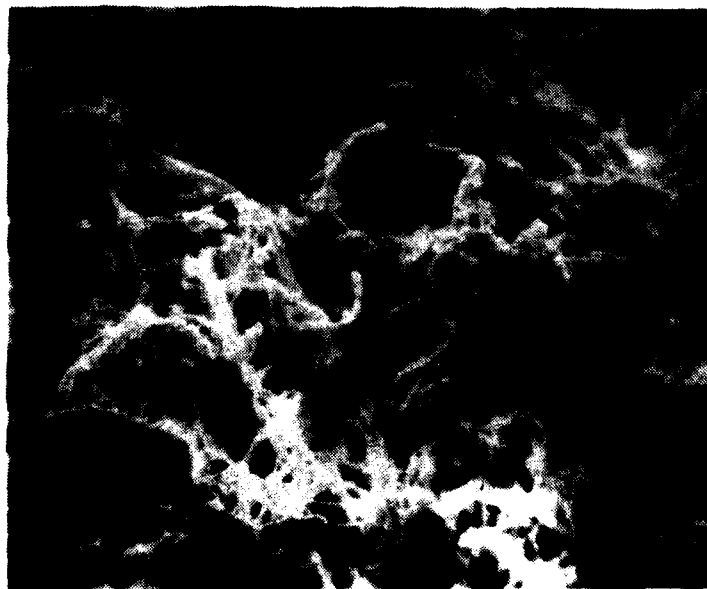


Figure 3. SEM Photograph of ISF Solution Agitation Material Which has been Subsequently Chopped.

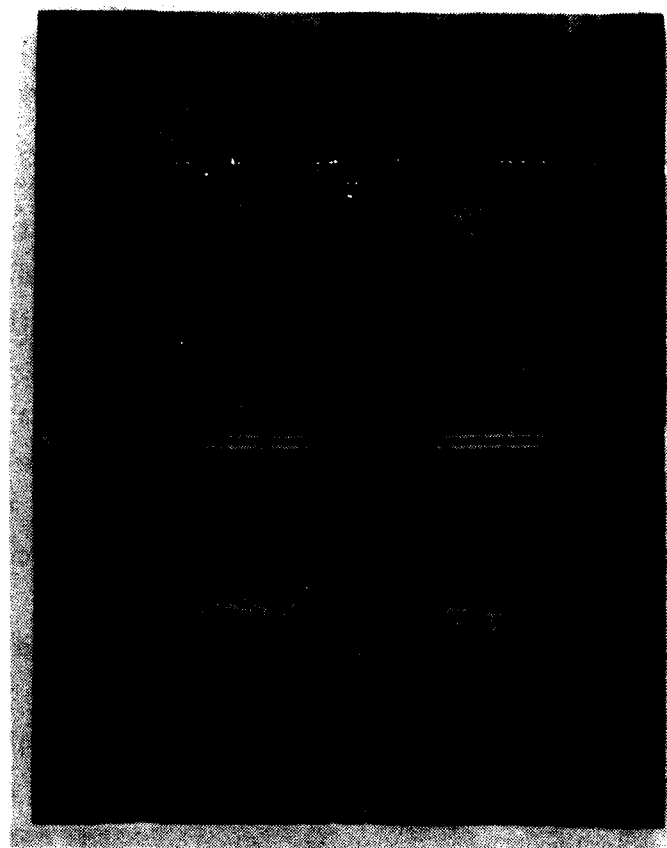


Figure 4. Regularly Spaced Tines Fiberized Via ISF. Magnification - 5X.

fibers in Figure 5. The high level of crystallinity and degree of molecular orientation is also shown in the X-ray diffraction pattern in Figure 6 by the sharp rings and pronounced arcs. Additional work with the wire configurations resulted in the formation of fibrous morphologies for several other polymers including isotactic polypropylene, poly-1-butene, and poly-4-methyl-1-pentene as shown in Figures 7 - 9, respectively. Although these materials did exhibit interesting structures as characterized by electron microscopy,

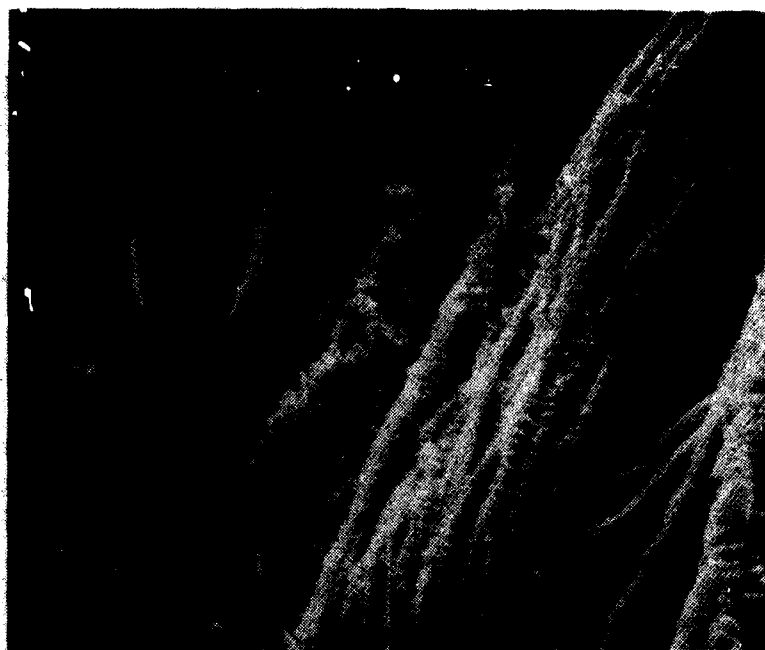


Figure 5. SEM Photograph of ISF Polyethylene Fibers.
Magnification - 100,000X.



Figure 6. X-Ray Diffraction Pattern Formed by ISF Poly-
ethylene Material.



Figure 7. SEM Photograph of ISF Polypropylene Material.
Magnification - 16,400X.



Figure 8. SEM Photograph of ISF Poly-1-Butene Material.
Magnification - 18,000X.



Figure 9. SEM Photograph of ISF Poly-4-Methyl-1-Pentene Material. Magnification - 9,500X.

thermal analysis and X-ray diffraction techniques, with the exception of isotactic polypropylene, no additional investigations were undertaken.

The polypropylene fibers produced via ISF processing appeared to be quite attractive due to their interconnected structure and strength as revealed in tensile testing²². As a consequence, they were investigated further in a program²³ to attempt to reinforce the encapsulant on a model high voltage component. One significant result of that program was the successful formation of the ISF material on the complex geometry part as shown in Figure 10. Even more significant was that Scanning Electron Microscopy and thermal analysis techniques showed the material to be essentially identical to the well



Figure 10. Electronic Component Before and After Fiberization.

characterized material produced in previous work. This meant that, through the appropriate manipulation of process parameters, in situ fibers could be formed reproducibly.

4. Fundamental Mechanism of Fiber Formation from Solution

A true understanding of all the molecular processes involved in in situ fiberization and the effect of experimental variables on these processes is currently not possible. However, the literature does contain references which can aid in the construction of a qualitative description of the mechanism of fiber formation. In particular, the oscillating bob experiments of McHugh¹⁹ demonstrated two things. First, elongational flow was necessary to induce fiber nucleation. Second, the crystallization process could be accomplished in an oscillating experiment. Typical cycling frequencies of 10 - 20 Hz were used which can be compared to those around 50 Hz used in ISF processing. The crystallizing polymer used in this work was polyethylene and the product after

washing was characterized as classical shish kebab material. The hypothesis was that an individual traverse of the bob or, one half cycle, was sufficient to form critical sized bundle like nuclei which then grew spontaneously into fibrillar crystals.

Additional information can be garnered from experiments conducted by Mackley²⁴ in which a wire gauze was rotated in a crystallizing solution of polyethylene at 20 rpm. The flow was laminar throughout, but did have regions with longitudinal flow gradients which developed in front of and directly behind the wire strands. The hydrodynamics encountered in Mackley's experiments were very similar to those which have been used in ISF processing^{18,19}. It is therefore safe to conclude that it is indeed the elongation flow component which induces nucleation of oriented fibers and any alteration in the process or substrate geometry which causes or enhances this type of flow is likely beneficial.

It is also necessary to consider crystallization kinetics when attempting to explain flow induced crystallization processes. It is well established that elongational flow is necessary to induce appropriate molecular orientation in solution, but the duration of this flow, as well as the magnitude of the velocity gradient, is important. In particular, the deformed molecules need a finite amount of time to be incorporated into the stable nucleus structure. If the flow period is insufficient this will not occur. This could explain why extremely high frequency ISF agitation experiments have been unsuccessful. Also, it is expected that molecular structure would be important in that molecules less prone to efficient packing could require additional time or stronger flow fields to adopt a configuration suitable for crystallization.

One additional formation mechanism which is particularly apropos to the present program is one put forth by McHugh and coworkers^{25,26} and also by Williamson and Busse²⁷. A schematic of the process is shown in Figure 11.

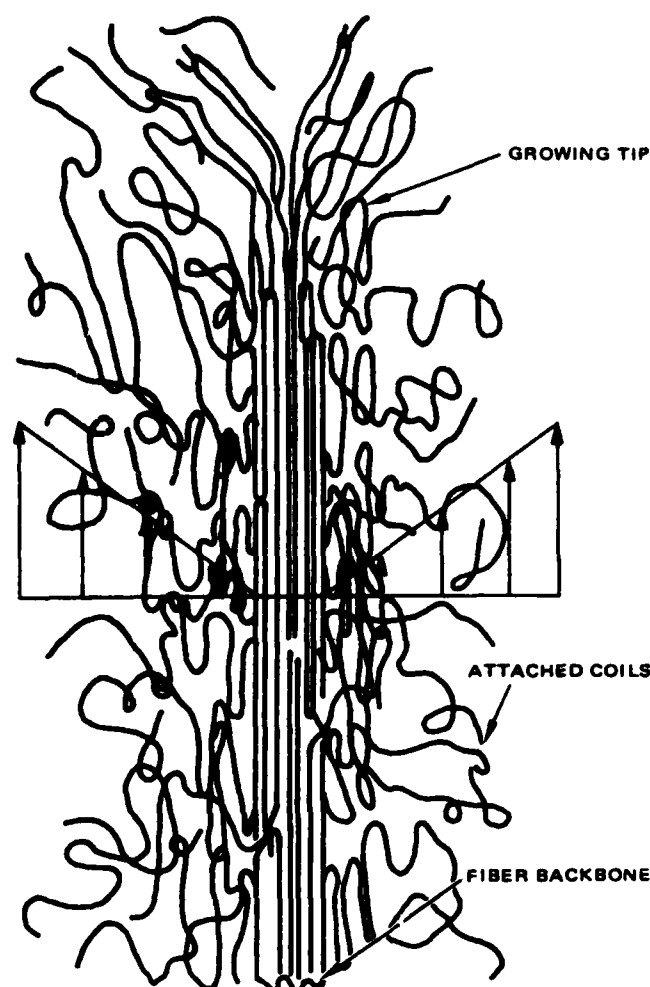


Figure 11. Entangled Fibers Crystallized into an Oriented State Via Shear Field Influence.

It assumes that polymer molecules, once partially attached in a critical size nucleus of oriented chains, will be reeled in to participate in that oriented morphology as a result of the simple shear flow gradients imposed by fluid motion past the nuclei. In the context of the present investigation, if molecules can be entrapped in the pore structure and induced to form nuclei or fibrils, then the above mentioned mechanism could come into play to produce oriented, and therefore strong, fibers extending out from the surface of the pore structure.

In summary, the interaction of the crystallizing species with the induced flow field is extremely complex. It is clear a high level of molecular orientation in solution is necessary to form initial nuclei and this can only be provided by elongation flow. It is also clear that this flow field must be applied for a sufficient amount of time to promote oriented crystallization. In an oscillatory experiment such as ISF processing, this means an appropriate balance between frequency and amplitude is critical. However, no definitive information is yet available on the quantitative effect of magnitude or duration of elongational flow on the kinetics of formation or the morphology of resulting fibrillar crystals.

SECTION II EXPERIMENTAL

1. Material

Isotactic polypropylene was selected as the fiber forming material in this work because of its propensity to form a network structure with good mechanical integrity²². The polymer was obtained from Amoco Chemical Corporation and the results of molecular weight characterization by gel permeation chromatography are shown in Figure 12. The solvents used in the fiberization process were reagent grade mixed xylenes and spectral grade methanol and acetone.

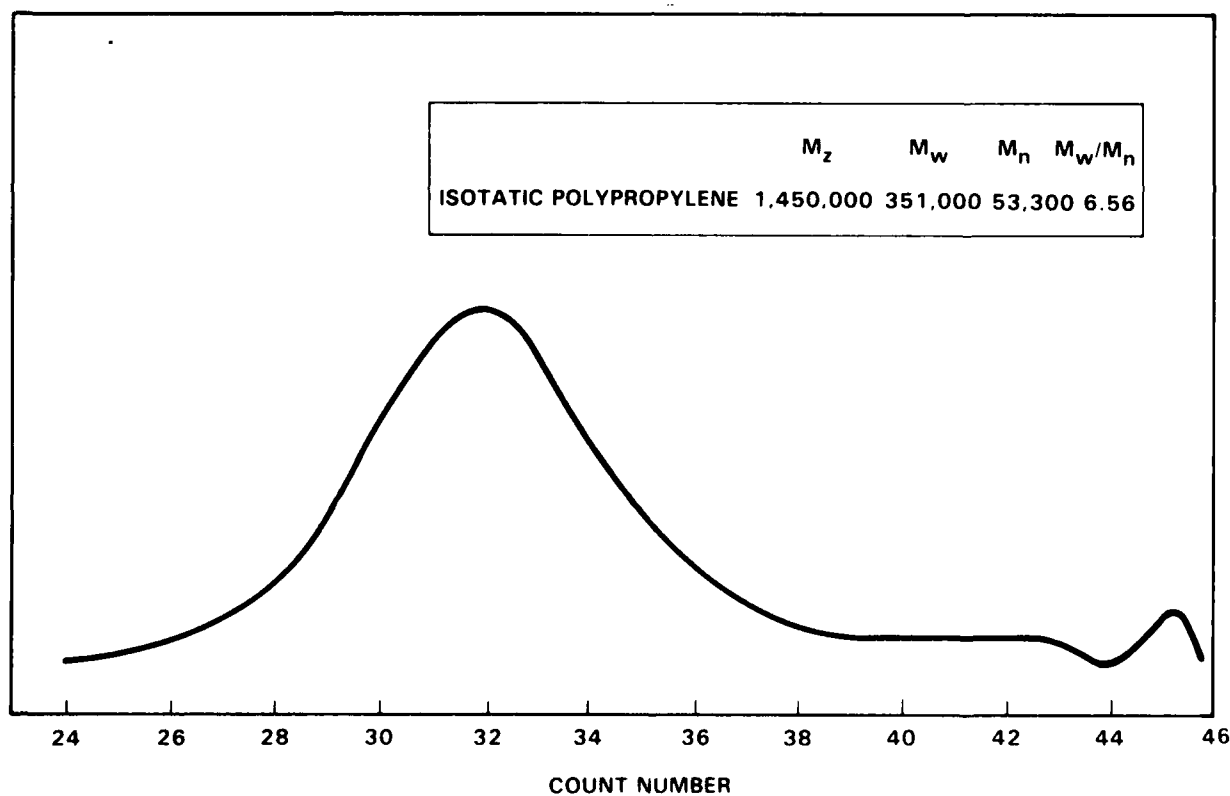


Figure 12. GPC Trace for Isotactic Polypropylene.

Two adhesive systems were investigated in this work. The first was FM-73, a 121°C cured bisphenol epoxy system with a latent amine catalyst and modified with nitrile rubber. The material was obtained from American Cyanamid as a film adhesive with a polyester mat carrier, designated FM-73, and without a polyester mat carrier, designated FM-73u. Both types were stored at subambient temperatures prior to use to avoid undesired advancement of cure.

The second adhesive, a brittle epoxy chosen for comparison with the FM-73, was an in-house formulation of Epon 828, obtained from Shell Chemical, Versamid 125, obtained from General Mills, and menthane diamine. The adhesive was formulated in the ratio of 100:21:13 parts by weight respectively and stored at subambient temperatures. Glass beads of two different diameters, 5 μm and 12 μm , were used to control the bondline thickness. Unless otherwise noted in the text, a cure schedule of two hours at 71°C was used for all the Epon adhesive materials.

2. Equipment and Procedures

The equipment used to conduct the fiberization experiments is shown in Figure 13. It consists of a large glass vessel filled with silicone oil which can be thermally controlled to $\pm 0.5^\circ\text{C}$. The thermostating fluid completely surrounds a smaller interior glass vessel in which the crystallization process takes place. An MB Electronics exciter/Ling amplifier/Hewlett Packard oscillator combination is used to drive and control the agitation. The specific procedures used to prepare samples will be discussed in the next section of the text. In general, the process involves agitating a substrate in a crystallizing polymer solution for a prescribed amount of time at a given temperature. This is followed by a washing step conducted in pure solvent (xylene) at a temperature usually $0^\circ - 5^\circ\text{C}$ above the ISF crystallization temperature. Agitation at low frequency, 5-10 Hz, is used to promote the process. Following washing, the xylene is extracted with solvents such as acetone and methanol and the sample is allowed to dry at room temperature.

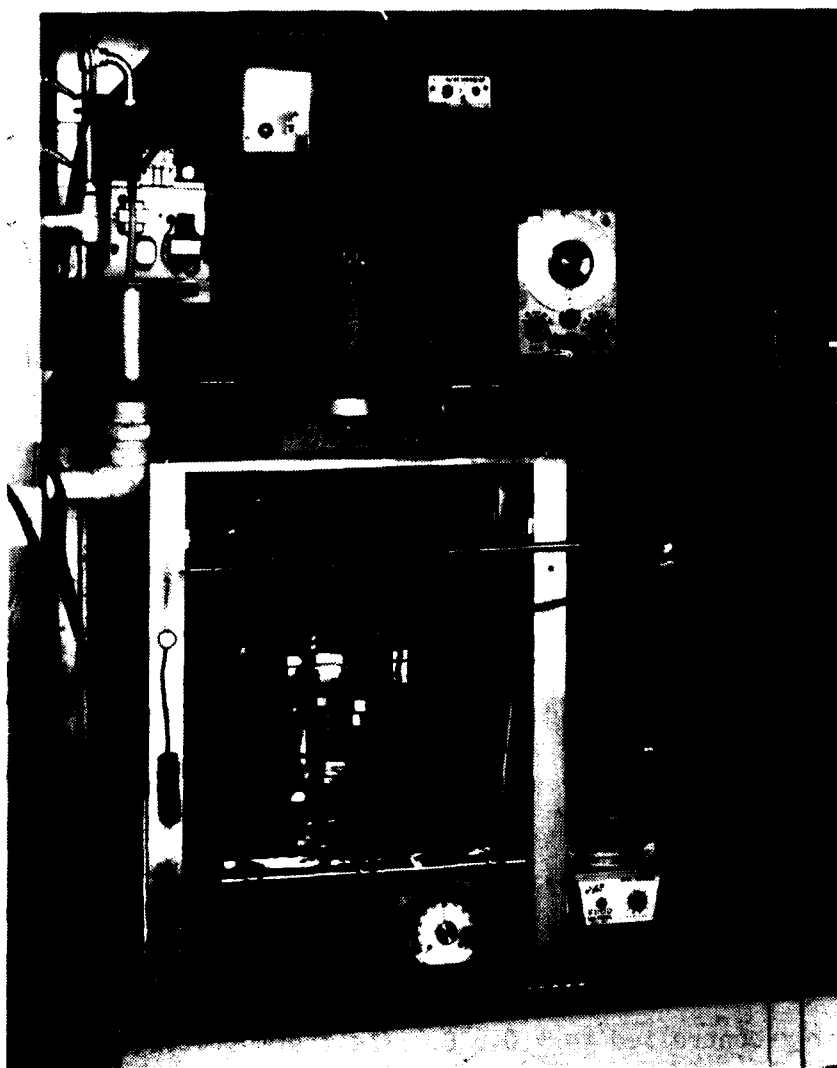


Figure 13. Apparatus Used For ISF Experiments.

The aluminum alloys studied in this work were 2024-T3 clad, 2024-T3 bare and 7075-T6 bare. Two specific treatments were used with these alloys; namely FPL etch and phosphoric acid anodizing. The chemicals and procedures used in these processes are detailed in a subsequent section of this report. The FPL etch was carried out in a standard tank designed for processing experimental samples. The vessel used for phosphoric acid anodizing treatments was an 11 liter pyrex container which was enclosed in a larger water bath to allow heating or cooling as required. Temperature control was maintained to $\pm 2^{\circ}\text{C}$. A filtered DC power supply was used for anodization and the upper operating range was 32 volts DC at 25 amperes.

A substantial portion of this program was dedicated to the treatment of the in situ formed fibers to enhance wetting and interaction with the adhesive systems used. One technique involved the use of a Tesla coil, capable of producing 30×10^3 volts, for corona discharge treatments. The tip of the coil was moved back and forth across the sample surface exposing each region for approximately 1 second. Bonding was then accomplished immediately following this treatment. A second fiber surface modification technique was plasma treatment, accomplished by the use of plasma etching equipment manufactured by International Plasma Corporation. A schematic drawing of the equipment is shown in Figure 14. The apparatus was equipped with a cylindrical quartz chamber (13 cm diameter, 34 cm length), a radio frequency power supply capable of supplying 300 watts, and a Varian pressure gauge capable of measuring pressures down to one micron of mercury. Gas flow rate was monitored and controlled with a Matheson 610 flowmeter. Calibration data on gas flow rates were obtained from Matheson for oxygen and helium, two of the gases used. No data were available for acetylene, the other gas used, so a behavior similar to ethylene was assumed and flow rates were determined accordingly.

The procedure used involved isolating each sample in the chamber followed by chamber evacuation to 30 microns and purging with the treatment gas for approximately 30 minutes. Treatment consisted of adjusting the RF power and maintaining proper gas flow for the designated exposure time. When chamber pressure changes were noted due to gas polymerization (C_2H_2) or activated gas velocities, the final plasma equilibrium pressure was recorded. Following treatment, the chamber was purged and samples were bonded immediately.

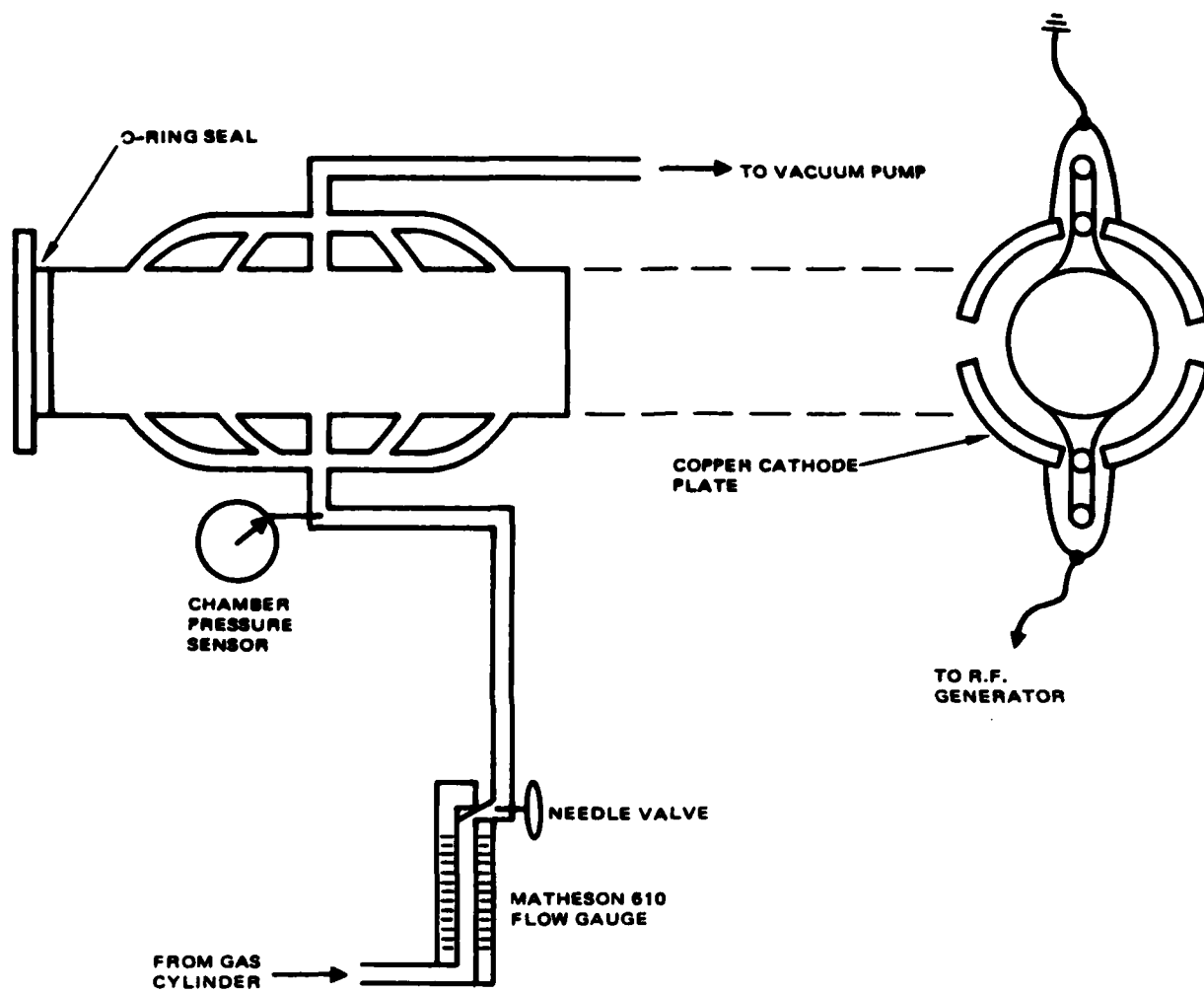


Figure 14. Schematic Drawing of Plasma Treatment Equipment.

SECTION III

RESULTS AND DISCUSSION

1. Aluminum Surface Treatments

The two surface treatments used in this work were FPL etch and the phosphoric acid anodizing process. The former is a widely used surface preparation developed by Forest Products Laboratory and detailed in Table 1. The second is also extensively used, but can be considerably more complex due to the greater number of experimental variables. Initial efforts in this area were concerned with reproducing known phosphoric acid anodizing technology.²⁸⁻³⁰ Specifically, conditions determined as optimum for adhesive joint durability were investigated. Table 2 shows the procedure and chemicals used to accomplish this.

TABLE 1
PROCEDURE FOR FPL ETCH

OPERATION	MATERIAL	PROCESS
Vapor Degrease or Solvent Wipe	1-1-1 Trichloroethane	
Etch	Deionized water 30 pbw 66° Be H ₂ SO ₄ 10 pbw Sodium Dichromate 1.5 pbw 2024 Aluminum .06 pbw	12 minutes 150-160°F
Rinse	Deionized water	2 minutes room temperature

TABLE 2
PROCEDURE FOR PHOSPHORIC ACID ANODIZING

OPERATION	MATERIAL	PROCESS
Vapor Degrease or Solvent Wipe	1-1-1 Trichloroethane	
Alkaline Clean	Oakite 61B	10 minutes
Spray Rinse	Deionized Water	5-7 minutes room temperature
Deoxidize	Nitric Acid/Amchem 6-16	15 minutes
	Amchem 6-16: 6-8% by volume 8-10% by weight	75-95°F
	Nitric Acid: 20 fluid oz/gal (70% HNO ₃)	
	Deionized Water: balance	
Spray Rinse	Deionized Water	5-7 minutes room temperature
Anodize	Phosphoric Acid	20-25 minutes room temperature
Spray Rinse	Deionized Water	5-7 minutes room temperature
Oven Dry	Circulating Hot Air	60 minutes, 130°F

It should be restated here that the initial objective was to produce acceptable anodic surfaces using optimized procedures already developed. The second thrust of this work was to extend this technology through appropriate parameter manipulation to produce surfaces compatible with the in situ fiberization process and at the same time retain suitable strength for adhesive bonding. It was assumed that concurrent with anodic layer thickness development would be an accompanying enlarging of the pore volume and that moving toward larger pore volumes would enhance fiberization.

The main process variables which can alter the character of the anodic layer formed are voltage, bath concentration and temperature, and anodizing time. The effect of these parameters on oxide thickness for 7075-T6 bare aluminum specimens is shown in Figures 15 - 17²⁸.

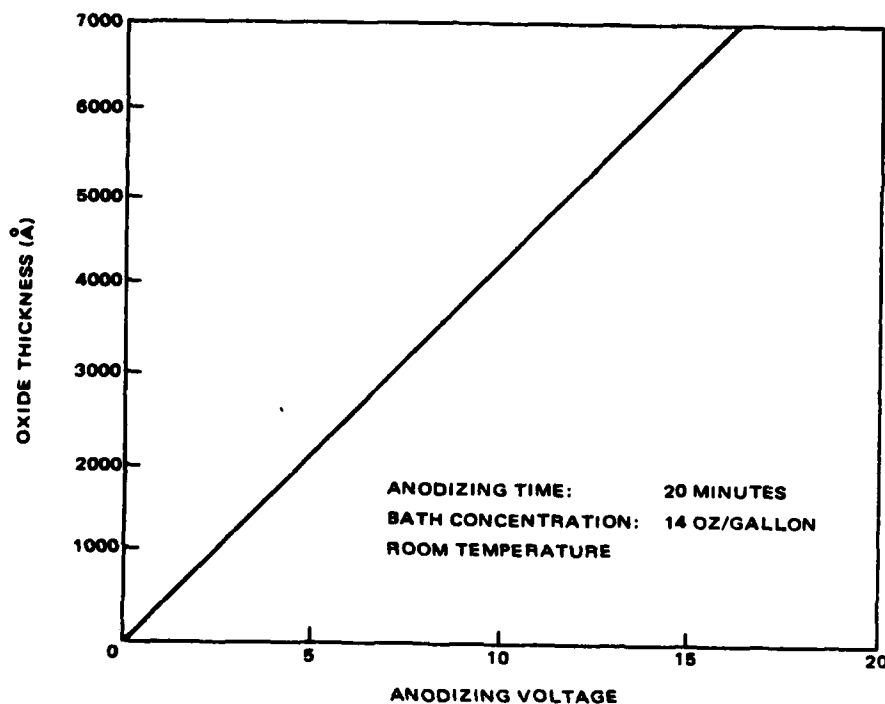


Figure 15. Oxide Thickness Versus Anodizing Voltage for Bare 7075-T6 Anodized in Phosphoric Acid.

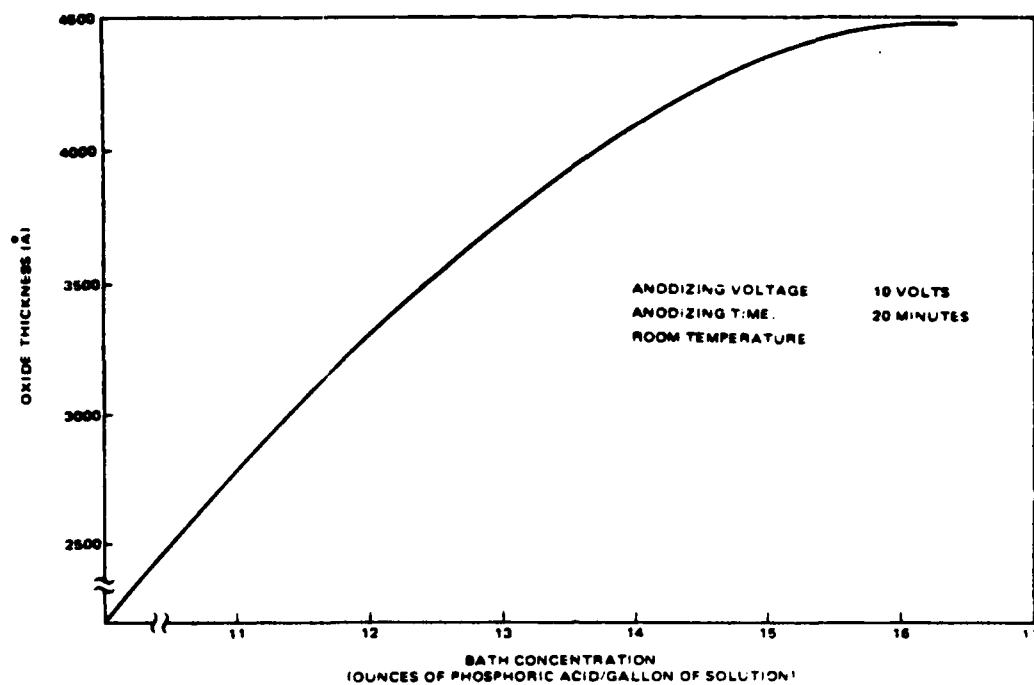


Figure 16. Oxide Thickness on Bare 7075-T6 Versus Concentration of Phosphoric Acid Anodizing Bath.

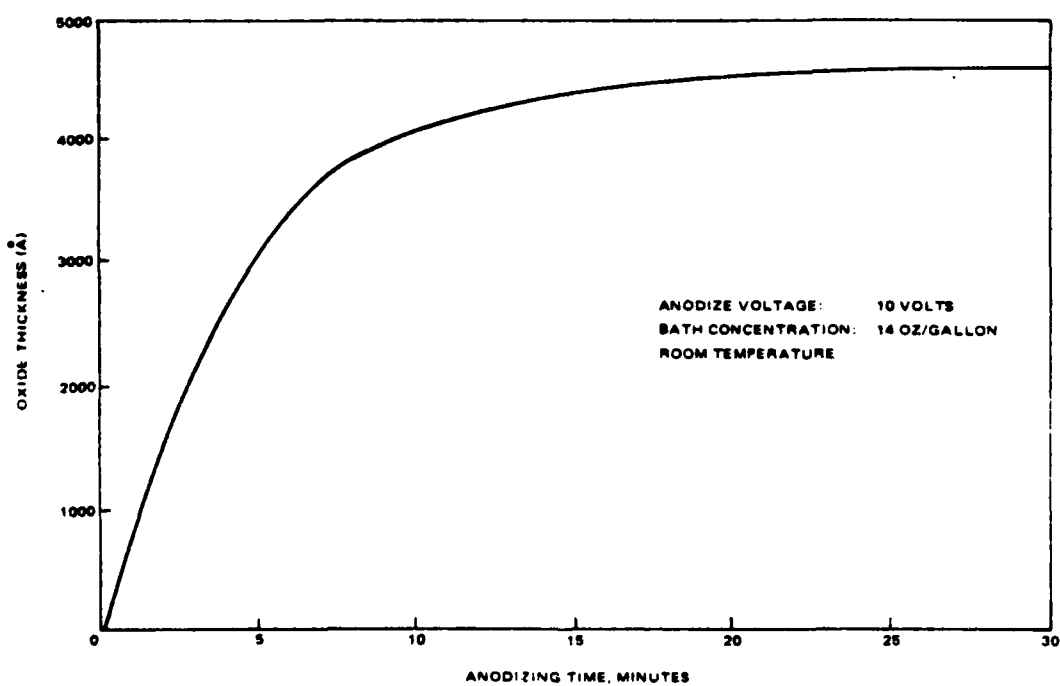


Figure 17. Oxide Thickness Versus Anodizing Time for Bare 7075-T6 Anodized in Phosphoric Acid.

It can be seen that anodizing voltage, and to a lesser degree, concentration do indeed impact oxide thickness while the influence of anodizing time appears minimal. The effect of temperature is not delineated in the literature and it was therefore chosen as the first parameter to investigate. The results of process temperature variation are shown in Table 3. The data generally show an increase in thickness with temperature for only the 2024-T3 clad samples, but it was felt this increase was essentially insignificant considering the experimental error involved in measurement and potential variances which would be noted if a statistical population were considered. As a consequence of these results, the study of temperature as a potentially useful variable to manipulate for anodizing process control was terminated.

It is useful at this juncture to discuss the technique used to evaluate anodic layer thickness. The measurement of anodic layer thickness and pore size is accomplished by treating a strip of aluminum .16 cm (.063 in.) thick and then bending the strip to crack the surface layer. The coating, thus exposed, is examined using Scanning Electron Microscopy (SEM). Pore size is determined by SEM observation of an intact anodized region. Typical examples of anodic layers are shown in Figures 18 and 19.

In addition to analyzing anodic layer thickness via SEM, it was also necessary to ascertain that the layer produced had the requisite strength. This was done using a procedure developed at Boeing called the wedge test. This procedure is well documented in the cited references^{29,31} and will not be explained here. The specific exposure conditions used in this work were 50°C and 95 percent relative humidity for one hour. The crack propagation distance and mode of failure were determined for the different adhesives used with different anodic layers produced by processing variable manipulation.

Continued phosphoric acid anodizing process development centered around the manipulation of voltage and anodizing bath concentration. Table 4 shows typical trends encountered when the voltage was increased.

TABLE 3
EFFECT OF PROCESS TEMPERATURE AND BATH
CONCENTRATION ON ANODIC LAYER THICKNESS*

MATERIAL	TEMPERATURE (°F)	CONCENTRATION OXIDE (OUNCES/GALLON)	THICKNESS (Å)
2024-T3 Clad	70	14	4500
7075-T6 Bare	70	14	2800
2024-T3 Clad	75	14	5500
7075-T6 Bare	75	14	2500
2024-T3 Bare	75	14	3000
2024-T3 Clad	80	14	5600
7075-T6 Bare	80	14	3000
2024-T3 Clad	85	14	6500
7075-T6 Bare	85	14	2900
2024-T3 Bare	85	14	2600
2024-T3 Clad	70	16	6100
7075-T6 Bare	70	16	3700
2024-T3 Clad	75	16	5800
7075-T6 Bare	75	16	3200
2024-T3 Bare	75	16	2900
2024-T3 Clad	80	16	5400
7075-T6 Bare	80	16	3200
2024-T3 Clad	85	16	5400
7075-T6 Bare	85	16	3300
2024-T3 Bare	85	16	3000

*Voltage - 10 volts, anodizing time - 22.5 minutes.



Figure 18. Anodic Coating on 2424-T3 Clad Sample.
Magnification - 24,000X.

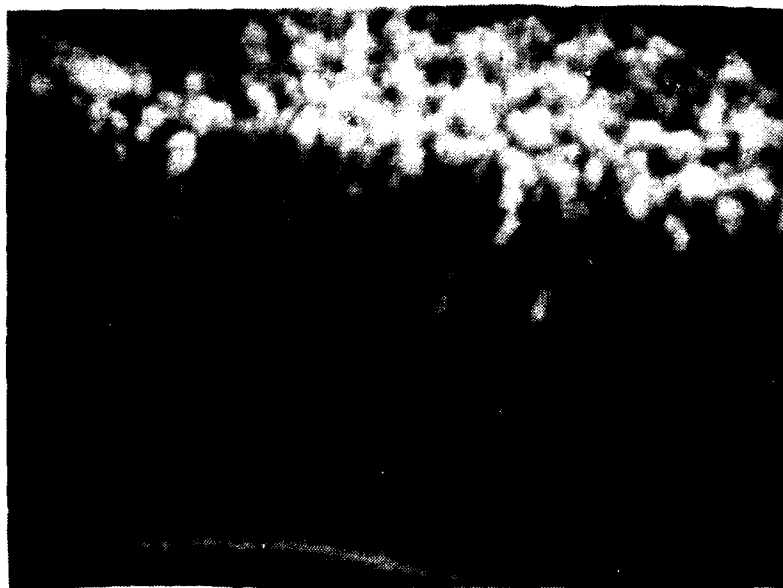


Figure 19. Anodic Coating on 2024-T3 Clad Sample.
Magnification - 24,000X.

TABLE 4
ANODIZED LAYER THICKNESS (IN Å) AS A FUNCTION OF VOLTAGE

ALUMINUM	ALLOY	10 VOLTS	20 VOLTS	30 VOLTS
2024-T3	Clad	6,500	15,000	32,100
2024-T3	Non-clad	3,100	3,750	4,200
7075-T6	Non-clad	2,900	3,800	4,000

These data reinforce the literature results previously displayed in Figure 16. The experimental setup used limited the voltage to 30 volts, but based on the coating thicknesses observed, this was deemed satisfactory. Concentration was also found to increase anodic layer thickness, but the effect was far less significant than that encountered by voltage manipulation.

It was stated previously that the pore size was measured by SEM examination. While this was satisfactory for grossly screening the effect of processing variables, it did not provide an accurate quantitative determination of size. Many techniques have been used to study pore dimensions but the most widely used is Transmission Electron Microscopy (TEM). One method, employed with some success³², is to section the oxide and view it directly. This requires a precision microtome and exacting technique. It offers the advantage, however, of looking directly at the specimen and eliminating certain experimental artifacts. The method used here involved a surface replication technique accomplished by chromium metal shadowing followed by the sputtering of carbon. The carbon replica was then viewed in the TEM. If sufficient care is taken, this technique offers similar quality results to the microtoming procedure. Typical TEM micrographs obtained are displayed in Figures 20 - 22, and show that the oxide structures are reasonably regular and the pore diameters are on the order of 600Å to 2000Å.

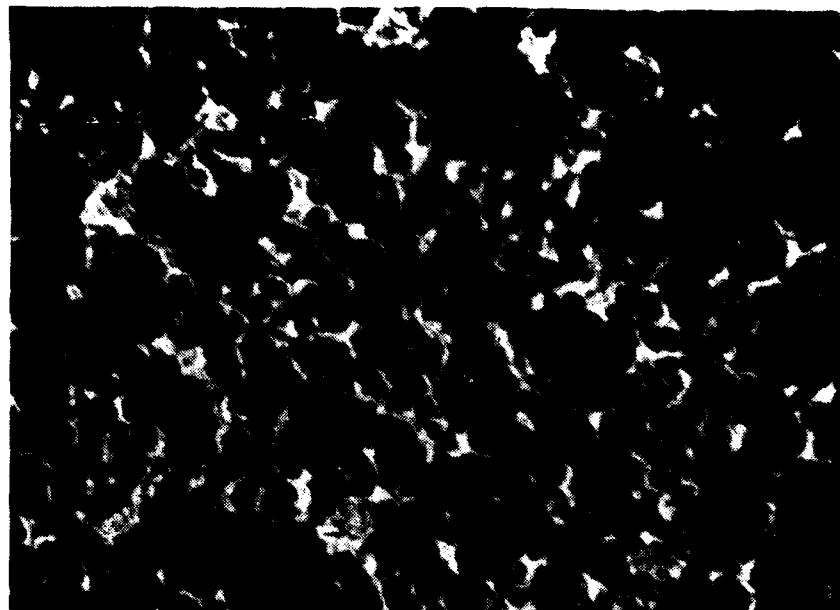


Figure 20. TEM Photomicrograph of Anodized 2024-T3 Clad Surface. Magnification - 80,000X.

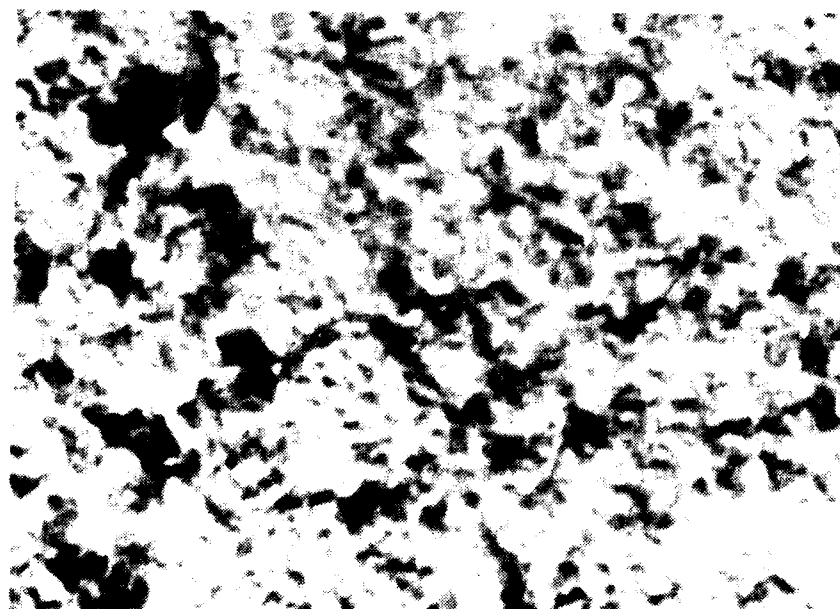


Figure 21. TEM Photomicrograph of Anodized 2024-T3 Bare Surface. Magnification 7,000X.

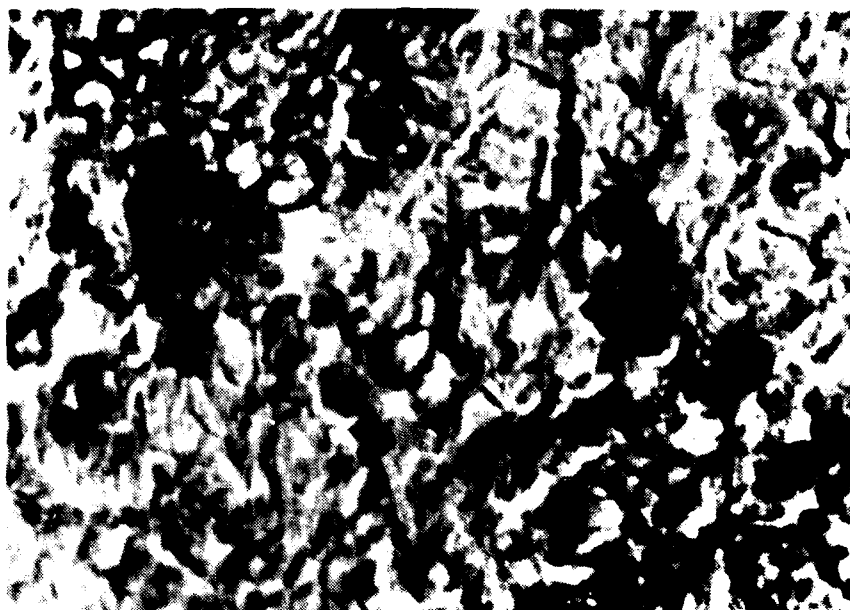


Figure 22. TEM Photomicrograph of Anodized 7075-T6 Bare Surface. Magnification - 80,000X.

After analysis of all the SEM and TEM micrographs and the wedge test data for specimens bonded with FM-73 and Epon 828, it was decided that the optimum anodic surface structure for fiberization was produced under the conditions shown in Table 5. This structure had pore dimension and anodic layer thickness deemed appropriate, while maintaining sufficient strength that wedge test failures were cohesive in nature.

TABLE 5

OPTIMUM PHOSPHORIC ACID ANODIZING CONDITIONS

Bath Temperature	25°C
Bath Concentration	20 fl/oz gallon phosphoric acid
Anodizing Voltage	30 volts
Anodizing Time	22.5 minutes

Two additional surface alteration procedures were undertaken on this program. It was thought that roughening the surface of the aluminum alloys prior to anodizing could possibly enhance the fiberization process. To this end, experiments were undertaken with a liquid honing technique. The surfaces of honed and nonhoned 2024-T3 clad specimens after anodizing are shown in Figures 23 and 24. The similarity of the two surfaces was initially surprising until it was determined that the scale of surface alteration via honing was orders of magnitude larger than the pore diameters produced by anodizing. Experimental limitations would not allow finer surface development and consequently further study of this technique was dropped. A second procedure involved the use of a surface etch developed at Hughes. It was successful in producing surface alterations on the order of 10 - 100 times the pore diameter without significant optimization. Typical etched surfaces are displayed in Figures 25 - 27. After some consideration, it was decided to cease investigation of the etch process due to its proprietary nature and the scientific purpose of this program. It has been mentioned because even the minor amount of work accomplished has led to some interesting conclusions which will be discussed later in the text.

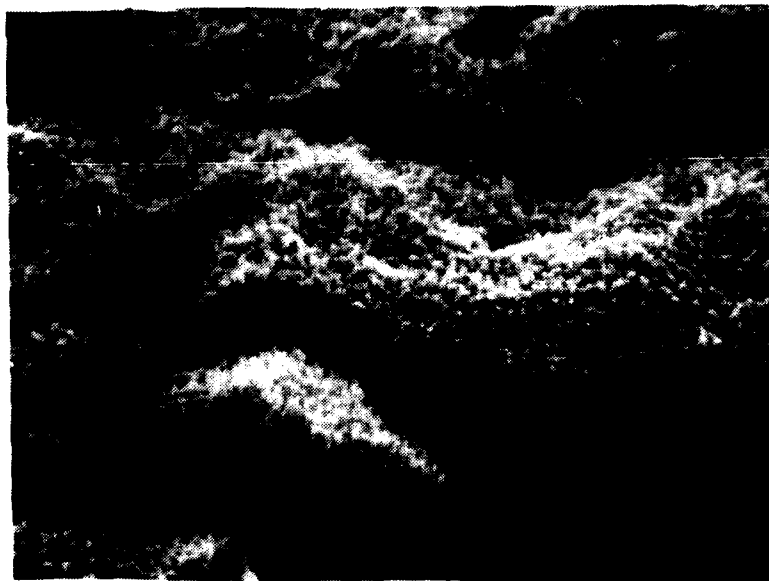


Figure 23. SEM of Anodized, Liquid Honed 2024-T3 Clad Surface. Magnification - 6,000X.

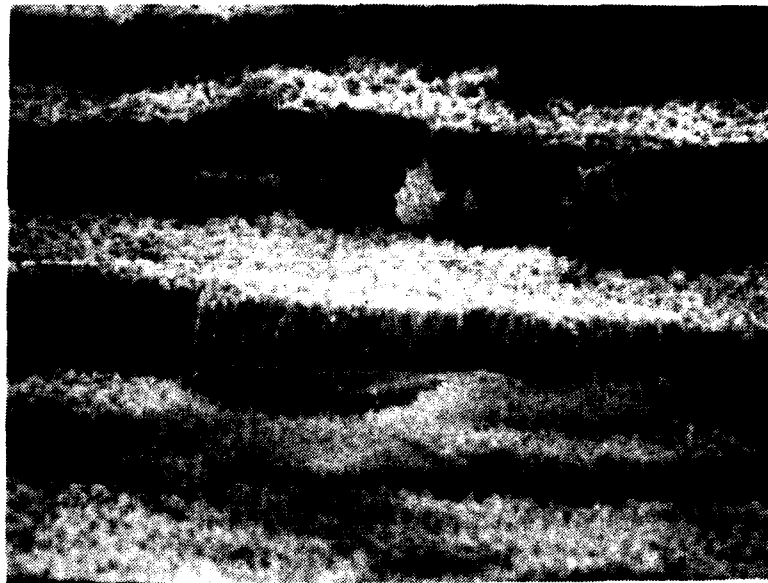


Figure 24. SEM of Anodized 2024-T3 Clad Surface.
Magnification - 6,000X.

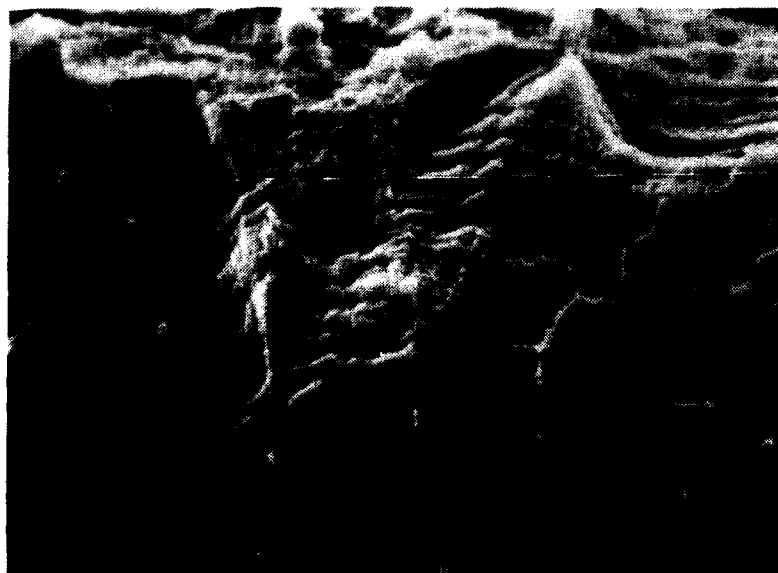


Figure 25. SEM of Etched 2024-T3 Clad Surface.
Magnification - 6,400X.



Figure 26. SEM of Etched 2024-T3 Clad Surface.
Magnification - 14,000X.



Figure 27. SEM of 7075-T6 Bare Surface.
Magnification - 24,000X.

2. Fiberization Optimization

In order to accomplish the goals of increased resistance to peel and reinforcement of the adhesive adjacent to the anodic layer it was thought necessary to produce in situ fibers with three distinct characteristics. First, the fibers should be of suitable size to form or deposit in the pore structure. Second, the aggregation of entangled fibers should extend some distance above the anodic layer surface and maintain a porous fibrous structure which is penetrable by the adhesive. Finally, this structure must be uniformly deposited across the test specimen dimensions. Based on the results of previous work^{22,23,33}, an experimental plan was devised to tackle the above stated objectives.

It has been shown repeatedly^{23,33} that oscillation frequencies in the range of 50-60 Hz have proved most fruitful for in situ fiber production. It was therefore concluded that 54 Hz would be used throughout this experimental program. The amplitude of oscillation in all previous work had been 0.53 cm and this was chosen for initial experiments. An experimental setup was constructed which allowed amplitudes as high as 1.20 cm and in later work, larger amplitudes of oscillation were investigated. This will be discussed in more detail in subsequent sections of the text. The remaining experimental variables of temperature and concentration were investigated according to the matrix shown in Table 6. One significant variable has been omitted from Table 6 and

TABLE 6
EXPERIMENTAL VARIABLE INVESTIGATION

		Polypropylene Concentration			
		.5%	1%	2%	5%
Temperature	95°C			*	*
	100°C				
	105°C				
	110°C	*			

* Did not attempt

that is fiberization time. In situ fiberization is a kinetic process and the normal method of selecting the appropriate experimental variables is to get formation of a reasonable amount of fibers in a prescribed time. The time period in this work was chosen as 1 hour.

One of the first conclusions reached after initial experiments were completed was that there was a marked difference in the efficacy with which the three different alloys could be fiberized, even under seemingly identical experimental conditions. This is shown in Figures 28 - 30. Two potential explanations of this phenomenon were postulated. First, each alloy contains a slightly different mixture of metallic components and it was thought that possibly one constituent present in one alloy and not another could act as a nucleating agent preferentially inducing fiberization. Subsequent experimental and literature investigations have shown this to be somewhat unlikely.³⁴ Second, the difference in surface topology, as shown in Figures 31 - 33, could induce flow field disruptions promoting or retarding fiberization. It can be seen that the most porous surface morphology is associated with the 2024-T3 clad specimens which are also the most easily fiberized. A definitive understanding here required investigation beyond the scope of this program. A decision was made at this juncture to concentrate on effectively fiberizing the 2024-T3 clad alloy specimens and, if resources allowed, to return to the other materials later in the program.

It had been observed in previous studies²³ that an increase in concentration or a decrease in temperature tended to cause fiber agglomeration and ultimately film formation on a microscopic scale. This was also observed in this work and is shown in Figure 34. In fact, to produce distinct fibers of diameters comparable with pore dimensions and in sufficient quantities, it was necessary to go to multiple fiberizations. Multiple fiberizations are simply consecutive fiberization treatments where, at the end of a given time interval, a fresh polymer solution is introduced to replace the original solution. Multiple fiberizations are generally conducted at higher temperatures with dilute solutions;



Figure 28. SEM Micrograph of Fiberized, Anodized 2024-T3 Clad Surface. Magnification - 6,500X.



Figure 29. SEM Micrograph of Fiberized, Anodized 7075-T6 Surface. Magnification - 6,500X.

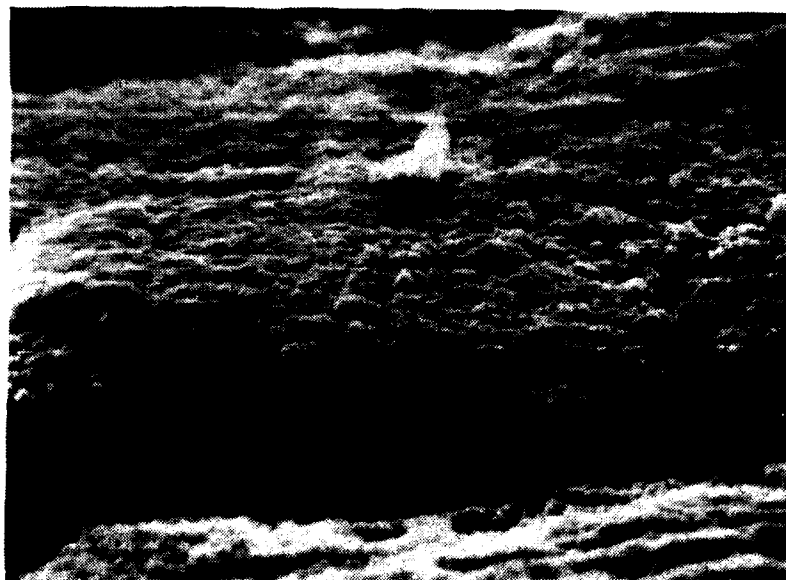


Figure 30. SEM Micrograph of Fiberized, Anodized 2024-T3 Bare Surface. Magnification - 6,400X.

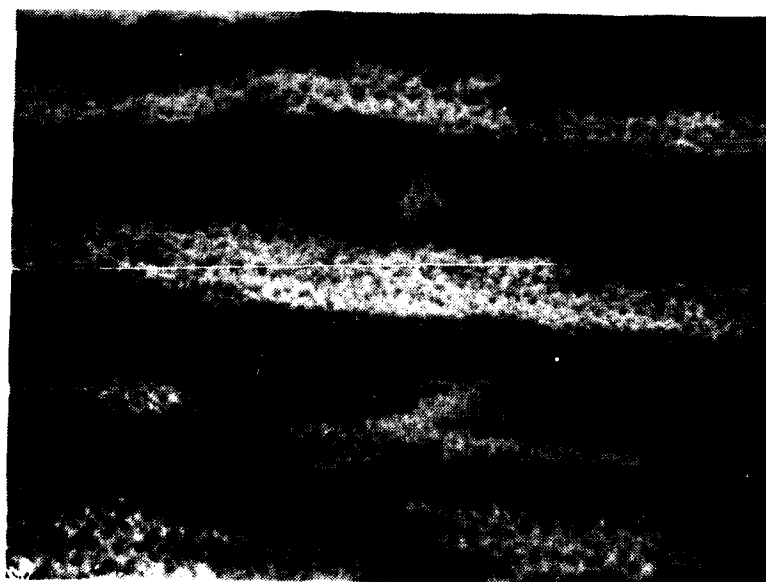


Figure 31. SEM Micrograph of Anodized 2024-T3 Clad Surface. Magnification - 6,000X.



Figure 32. SEM Micrograph of Anodized 7075-T6 Surface. Magnification - 6,500X.

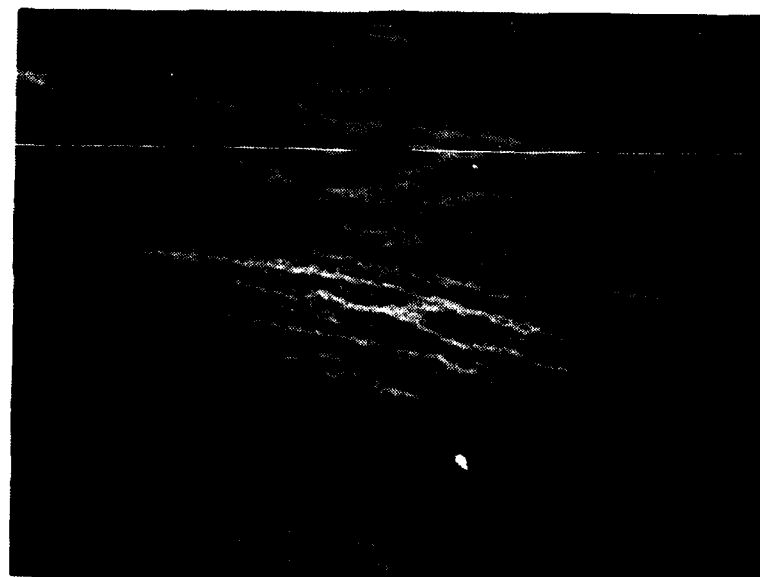


Figure 33. SEM Micrograph of Anodized 2024-T3 Bare Surface. Magnification - 6,000X.



Figure 34. SEM of Fiberized Anodic Surface Showing Film Formation. Magnification - 6,400X.

that is, polymer concentrations below 1 percent weight polymer/volume solvent. As alluded to above, this technique usually results in fibers with smaller diameters. It is not clear at this juncture whether the individual fibers are indeed smaller using this technique or these methods (higher temperature, lower concentration) reduce the driving force for crystallization and the self nucleation of fiber on fiber growth which leads to agglomeration and correspondingly larger fibers. It is clear, however, that this technique allows controlled fiber buildup over time without associated film formation. Figure 35 shows the result of multiple fiberizations and can be compared to Figure 28 for a single fiberization conducted under identical experimental conditions.



Figure 35. SEM Micrograph of Fiberized, Anodized 2024-T3 Clad Surface Subjected to Multiple Fiberizations. Magnification - 5,000X.

Multiple fiberizations were investigated at different temperatures (100°C , 105°C) and concentrations (.25 to 1.0 percent). It was observed that at the lower concentrations, the growth of fibers was quite slow and it could take as many as 6 - 8 distinct treatments to produce a fiber mass which was on the order of 1 mm thick. It was not known at this point what represented a reasonable amount of fibrous deposition. Therefore, a decision was made to consider two levels of fiber buildup. The first condition, termed lightly fiberized, was produced by a 1 hour fiberization at 100°C from a 1 percent polymer solution. The second condition, termed heavily fiberized, was produced by an initial 1 hour fiberization at 100°C from a 0.25 percent polymer solution, followed by 1 - 3 sequential fiberizations at the same temperature but with a 2 percent polymer solution. In each case, the samples were exposed to solvent washing $0 - 5^{\circ}\text{C}$ above the processing temperature after fiberization to remove any polymer in the solution trapped in the fibrous network which could precipitate as a film after solvent evaporation.

The fiberization discussion presented so far has been concerned with forming a suitable fiber mass composed of individual fibers with diameters compatible with pore dimensions. The question of whether fiber formation does occur in the pores themselves or simply on the anodic coating surfaces has not been addressed. Photomicrographs such as Figure 35 indicate that there may well be a considerable proportion of each type of growth. Figure 36 shows fibers emanating from the middle and bottom of the anodic layer but none stretching from surface to surface. Perhaps Figure 37 is the most enlightening of all. Here fibers seem to extend from the interior of the anodic layer to a dense fibrous mat formed directly above the anodic surface. This, in essence, is the exact structure desired for mechanical interlocking and reinforcement. Based on these micrographs and others not presented here, it was the opinion of the authors that there is indeed some fiber formation in the pores of the anodic layer. It was thought, however, that growth in the pores was not extensive and that methods outside the manipulation of standard fiberization parameters should be investigated to increase this type of growth.

Two techniques were attempted to accomplish this. The first was to attach a conductive member to the aluminum coupon and remove heat through this member during fiberization. This would, in principle, reduce the temperature of the coupon with respect to the supercooled polymer solution and induce preferential crystal nucleation and growth in the pores rather than in the fluid near the anodic layer surface. Several experiments were undertaken but, based on SEM micrographs, no appreciable changes in fiber growth patterns were noted.

The second concept studied involved the use of silane coupling agents. It was envisioned that an appropriate silane molecule could be selected such that one end of the chain would be attracted to the aluminum oxide anodic layer while the other end would be compatible with the organic crystallizable polymer. Several different compounds were investigated including vinyltrichlorosilane, octadecyltriethoxysilane, and vinyltriethoxysilane. A Fourier Transform Infrared (FTIR) technique was developed to detect the presence of silane on the aluminum coupons and used to optimize treatment process parameters. Two major difficulties were encountered during experimentation. First, with some of the more unstable



Figure 36. SEM Micrograph of Lightly Fiberized,
Anodized 2024-T3 Clad Surface.
Magnification - 5,000X.

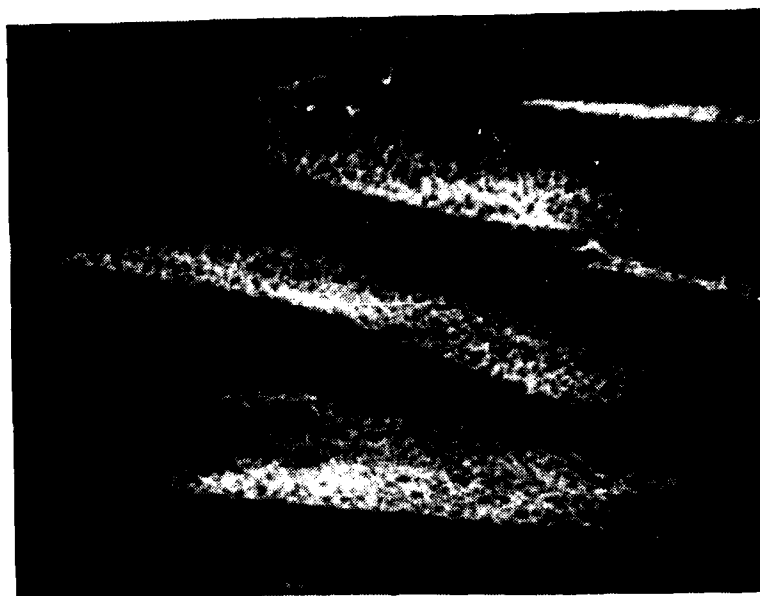


Figure 37. SEM Micrograph of Heavily Fiberized,
Anodized 2024-T3 Clad Surface.
Magnification - 5,700X.

materials such as the vinyltrichlorosilane, polymerization was found to occur. This resulted in thick pore filling deposits which were inappropriate to induce the type of behavior desired. The second difficulty was that the less reactive materials did not remain attached to the aluminum after exposure to 100°C xylene. It was felt, even after these difficulties, that experimental techniques could be worked out to explore the coupling concept. However, the resources remaining for this program did not permit such an investigation.

3. Fiber Surface Treatments

It is well known that the incompatibility of many adhesive materials with polyolefins has required the use of adhesion promoting treatments. In previous in situ fiber studies²³, there were some indications that interaction between the epoxy encapsulants and the polypropylene fibers could be improved. Specifically, under extreme thermally induced stresses, cracks were noted in fiberized specimens which seemed to run along sheetlike layers of fibers. The conclusion drawn from this was that the fiber-matrix interface was the weak point in the composite system. Although not considered in the original experimental plan, it was, during the course of this program, deemed appropriate to explore techniques to enhance fiber-adhesive matrix adhesion. Several general approaches were considered including acid etched, chemical modification of the polypropylene molecular structure and plasma and corona surface treatments. Chemical modification and the use of acids were eliminated due to complexity of effort required and potential damage to the anodized aluminum, respectively. It was therefore decided to investigate plasma and corona discharge techniques.

The application of high frequency voltage potentials to a gas results in activated gaseous molecules which are commonly called plasmas if low pressure (≤ 3 Torr) are used and corona discharge if atmospheric pressures are used. These activated gases may exist in metastable energy states and as ions or free radicals³⁵. In a proper sense, the term plasma refers to positive ions and free electrons produced by high energy ionization. However, the literature also commonly refers to low pressure electrodeless radio frequency discharges as plasmas and in the context of this work, the term will refer only to such electrodeless discharges.

It is well known that plasma and corona treatments have been successful in promoting adhesion to polymer surfaces although there remains some disagreement concerning the mechanism of adhesion enhancement. A variety of factors have been proposed including improved cohesion of the surface polymer skin³⁶, increased surface roughness and surface area, a change in surface energy due to the addition of polar groups to the polymer, the removal of weak surface layers by oxidation, and surface cleaning by removal of adsorbed material³⁵. Plasma gases such as oxygen have been shown to increase the surface crosslinking of polyolefins such as polyethylene, and similar results have also been observed using activated noble gases such as helium. This latter technique has come to be known as CASING (Crosslinking by Activated Species of INert Gases)^{38,39}. Schonhorn and Hansen, the originators of the CASING technique, have shown crosslinking begins at the polymer surface and extends into the film as exposure is increased. They reported that crosslinking was found to extend 1000Å into a polyethylene film after exposure to plasma activated helium for only 5 seconds. This limited exposure was also correlated with maximum adhesion to an epoxy adhesive system. The conclusion drawn was that the increase in adhesion was due to the improved polymer cohesive strength as a result of the crosslinking. Other techniques were also used to achieve improved polymer strength without changing surface energy, and they also resulted in improved bonded joint strengths^{40,41}.

Plasma treatments with gases such as oxygen and nitrogen lead to changes in polymer surface energy and wetting and can also positively impact adhesion⁴². In fact, it is these factors, in the opinion of some researchers⁴³, which have resulted in the observed increased adhesion to polyolefin films. In other cases, increased adhesion to polypropylene induced by nitrogen corona discharge has been explained by a roughening of surface topology via ablation³⁷. This ablation resulted in the production of 500Å hemispherical mounds on the polymer surface. In cases where plasma treatments were concluded with polymerizable gases such as acetylene, increased adhesion has been attributed to surface topology produced by the deposition of the polymerizing species⁴⁴.

This condensed review of the literature has pointed up the fact that it is difficult to predict precisely the effect of a given plasma gas or corona discharge treatment on any given polymeric material, however, several treatments have been shown to be successful for adhesion of epoxy adhesives to polypropylene substrates. These include oxygen and helium plasmas and corona discharge exposures in air and nitrogen³⁷. Although it has not been applied to polypropylene⁴⁴, acetylene plasma polymerization also appears promising.

In order to appropriately evaluate the effect of the plasma and corona discharge treatments, it was necessary to design a well controlled experiment. To this end, sheets of polypropylene film were treated and then bonded to make a sandwich test sample as shown in Figure 38. Several factors have been shown to effect the results of plasma exposure to polymer films. These include the chamber pressure in which the reaction is conducted, the power density in the chamber and near the polymer surface, the time of exposure, and to a lesser degree, the flow rate of gas into the chamber. The equipment used limited the range of experimental capabilities. For instance, power was limited to 300 watts and vacuums of less than 20 microns were not possible. It was also not possible to accurately control gas flow rates to less than .25 SCCM (standard cubic centimeters per minute). Within these restrictions, the conditions which produced successful results in the literature studies cited were adhered to as much as possible. Corona discharge exposure was provided by the use of a Telsa coil. Some difficulty was encountered in using the coil due to the high voltages (30,000 volts) involved. In particular, sparking and localized melting due to overexposure were common. It was possible to reduce this considerably by using a layer of dielectric such as Mylar^(R) below the polypropylene film.

The results for the treated, bonded, and tested specimens are shown in Tables 7 and 8. It can be seen that, in general, the oxygen plasma treatments appeared the most promising from the perspective of adhesion enhancement. SEM micrographs were also taken of treated surfaces to attempt to elucidate more mechanistic information. When the surface of the untreated polypropylene film, as shown in Figure 39, is compared with the surfaces treated with oxygen

TABLE 7

SHEAR STRENGTH VERSUS TREATMENT CONDITIONS FOR
SAMPLES BONDED WITH EPON 828 ADHESIVE SYSTEM

Gas	Flow Rate (cm ³ /min)	Power (watts)	Pressure (Torr)	Time (min)	Shear Strength (lbs/in ²)
None	---	---	---	---	270
He	20	100	1.1	37	Not measurable
He	8.0	200	.34	30	320
O ₂	6.7	50	---	10	640
O ₂	3.0	50	.2	.5	170
O ₂	.8	50	.19	35	130
O ₂	.4	25	.2	.25	290
C ₂ H ₂	1.0	10	.03	9	600
C ₂ H ₂	.4	7	.03	5	710
Bondline reduced from 12 mils in above to 5 mils					
None	---	---	---	---	420
H ₂	.95	100	.24	30	820
O ₂	17	100	1.0	35	2850
O ₂	21	100	1.0	.05	2910
O ₂	.75	25	.12	20	410
C ₂ H ₂	.20	4	.04	5	601
Air	Corona discharge via Telsa Coil				1370

TABLE 8

SHEAR STRENGTH VERSUS TREATMENT CONDITIONS FOR
SAMPLES BONDED WITH FM-73 ADHESIVE SYSTEM

Gas	Flow Rate (cm ³ /min)	Power (watts)	Pressure (Torr)	Time (min)	Shear Strength (lbs/in ²)
None*	---	---	---	---	1040
None	---	---	---	---	580
He	20	100	1.1	37	Not measurable
He	8	200	.34	30	320
He	.95	100	.24	30	980
O ₂	6.7	50	---	10	550
O ₂	3	50	.2	.5	530
O ₂	.8	50	.19	35	720
O ₂	.4	25	.2	.25	860
O ₂	.75	25	.12	20	550
O ₂ *	21	100	1.0	.05	2280
O ₂ *	17	100	1.0	35	2450
C ₂ H ₂	1.0	10	.03	9	620
C ₂ H ₂	.4	7	.03	5	550
C ₂ H ₂ *	.2	4	.03	5	670
Air	Corona discharge via Telsa coil				1240

*Indicates adhesive used without mat carrier.

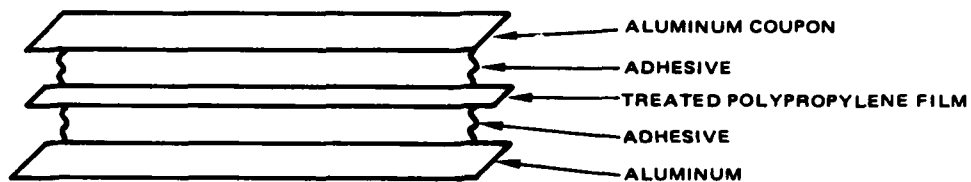


Figure 38. Sandwich Test Specimen Used With Polypropylene Film Plasma Studies.

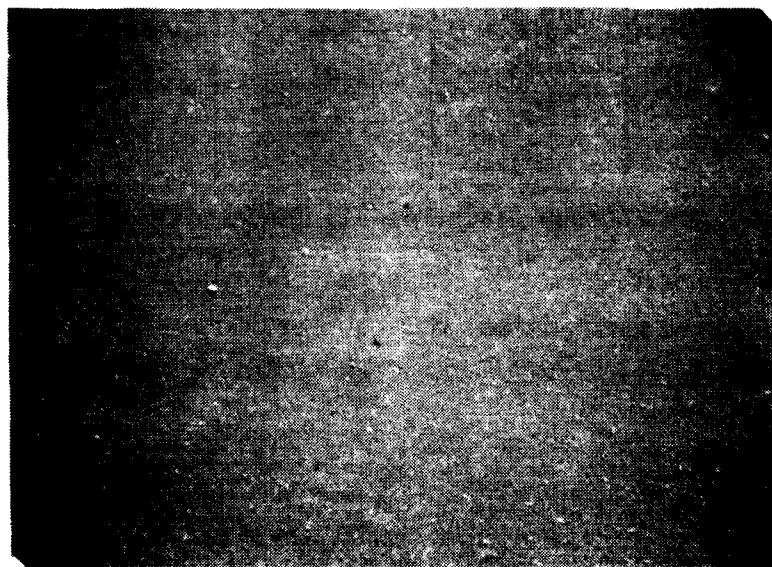


Figure 39. SEM Micrograph of Untreated Polypropylene Film Surface. Magnification - 5,000X.

plasma, as shown in Figures 40 and 41, it is clear that the surface is roughened by the thirty minute exposure, but remains topographically unaltered after three seconds of oxygen plasma exposure. In both cases, an increase in adhesion was observed and it is postulated that this is due to crosslinking of the surface skin and grafting of polar oxide groups onto the polymer. It is further postulated that the long exposure times resulted in considerable softening and even flow concurrent with the crosslinking reactions. Figure 42 shows the surface of a film treated with helium plasma. Again the surface is roughened as a result of the same processes occurring with the long time oxygen treatment. Figure 43 shows the surface of a film treated with acetylene. It appears that surface polymerization did indeed take place but unfortunately, this did not serve to drastically enhance the resultant bond strength.

All of the work done with polypropylene was conducted by exposing the film directly and then immediately bonding it between the anodized aluminum coupons. In the case of the in situ fibers, the plasma treatments had to be performed after the material was deposited on the coupons. This resulted in some experimental difficulties which are displayed in Figure 44. Here, the SEM micrograph displays melted and recrystallized fibers resulting from heating encountered during a 30 minute helium plasma exposure. Sample heating seemed to be enhanced by the presence of the aluminum coupons in the chamber and this fiber melting was typical of virtually all long time plasma treatments. Figure 45 shows fibers exposed to oxygen plasma for 3 seconds. Here, it appears the fiber morphology remains unchanged indicating heat buildup was insufficient to damage the deposited material. It should be pointed out at this juncture that it appeared clear the only plasma treatment (including corona discharge) which did not destroy the morphology produced during in situ fiberization was the short term oxygen exposures. Nevertheless, it remained a distinct possibility that, even though the original fibrous structure was altered during plasma treatment, some interesting data could be obtained by studying these altered materials in adhesively bonded specimens. Therefore, many of the treatments used with the polypropylene films were also investigated with fiberized specimens.

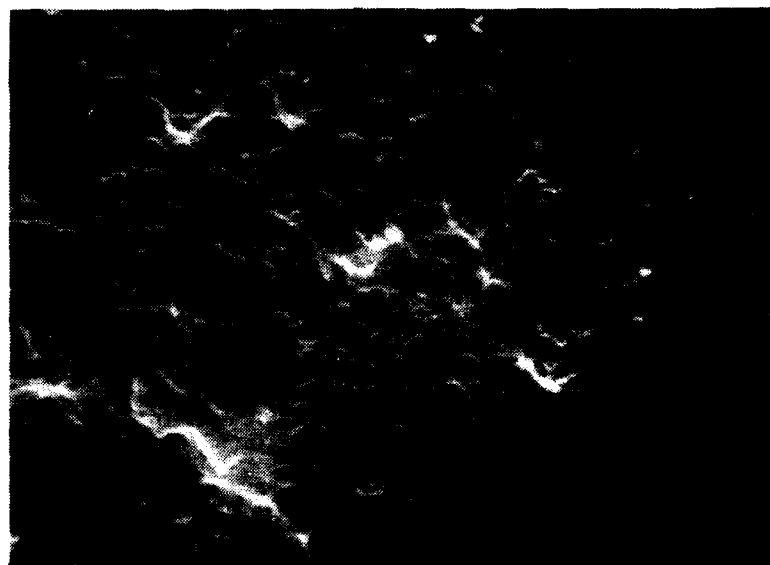


Figure 40. SEM Micrograph of Polypropylene Film Subjected to Extreme Oxygen Plasma Treatment. Magnification - 5,000X.



Figure 41. SEM Micrograph of Polypropylene Film Subjected to Mild Oxygen Plasma Treatment. Magnification - 5,000X.

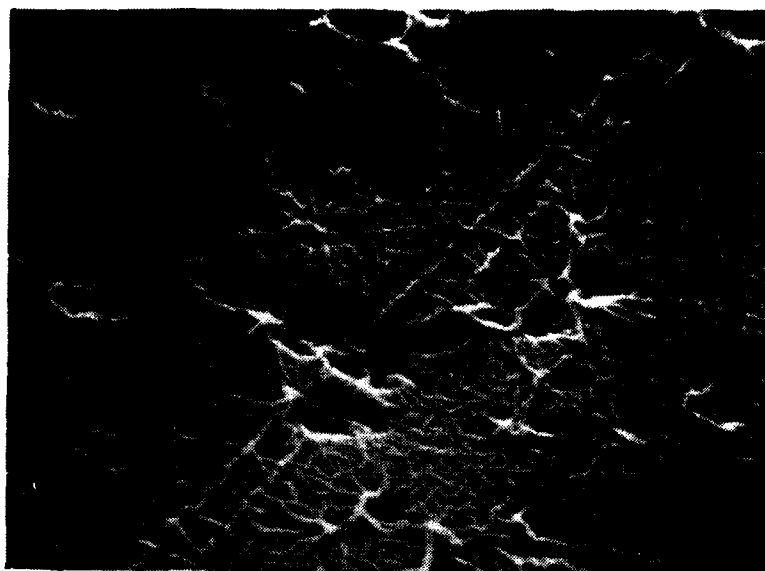


Figure 42. SEM Micrograph of Polypropylene Film
Treated With Helium Plasma.
Magnification - 5,000X.



Figure 43. SEM Micrograph of Polypropylene Film
Treated With Acetylene Plasma.
Magnification - 5,000X.

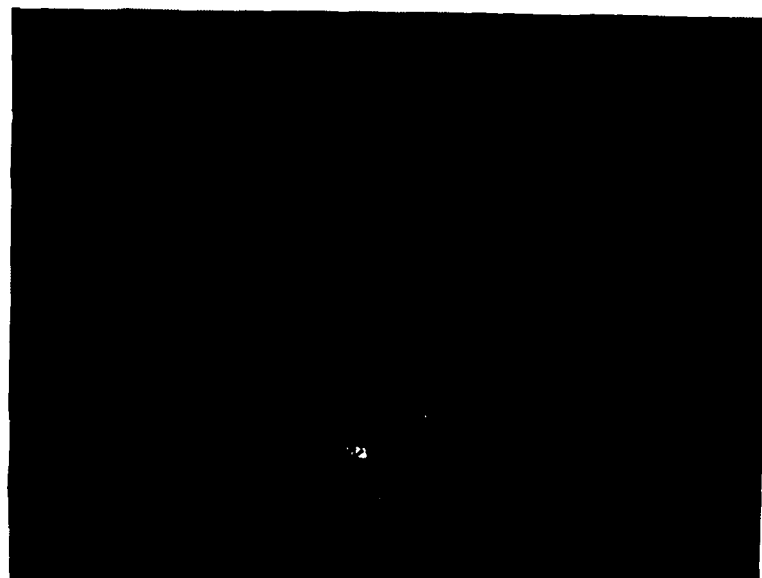


Figure 44. SEM Micrograph of Fiberized Specimen Subjected to Long Term Helium Plasma Treatment. Magnification - 4,500X.



Figure 45. SEM Micrograph of Fiberized Specimen Subjected to Short Term Oxygen Plasma Treatment. Magnification - 5,200X.

4. Property Determination and Analysis

Fiberized and treated specimens along with appropriate controls were tested in a lap shear and T-peel mode according to procedures outlined in ASTM D1002 and ASTM D1876, respectively. The results of this test program are shown in Tables 9-11. The majority of the data shown is for specimens bonded with FM-73u, the adhesive without the mat carrier. It should also be mentioned that this adhesive is normally used with a primer, designated BR-127. Both the mat carrier and the use of a primer were eliminated from consideration here to reduce the complexity of data interpretation; that is, the objective of the program was to evaluate the benefits of in situ fibers in the simplest system possible.

The data in Tables 9 and 10 for FM-73 lead to some interesting conclusions. First, the lap shear and T-peel data indicate that, in general, a heavily fiberized specimen has greater strength than a lightly fiberized specimen. Second, the plasma treatments were generally effective in increasing strength of the fiber containing bondlines. Finally, the performance of the anodized control specimens was generally better than that of the fiberized specimens; the best fiberized specimen performance being observed after oxygen plasma treatments. The results for the Epon 828 adhesive system shown in Table 11 follow the same general trends.

While these mechanical results may not appear totally encouraging, it is necessary to study the micrographs of the failed samples to elucidate the reason for the observed performance. It generally appears that more than one failure inducing factor is occurring with respect to the polypropylene-adhesive resin interaction. The first of these factors is polypropylene film formation and adhesive debonding. Film formation has been alluded to earlier in this report and is well depicted in Figure 46. The lack of protrusion of distinct fibers or a fiber mat results in a weak interface, even though the surface of the

TABLE 9

SHEAR STRENGTH AND PEEL STRENGTH FOR LIGHTLY FIBERIZED
COUPONS BONDED WITH FM-73 ADHESIVE SYSTEM

GAS	FLOW RATE (cm ³ /min)	POWER (watts)	PRESSURE (torr)	TIME (min)	LAP SHEAR STRENGTH (lbs/in ²)	T-PEEL STRENGTH (lbs/in.w)
---	---	---	--	--	870*	7*
He	.95	100	.8	30	---	9*
O ₂	21	100	1	.04	---	9*
O ₂	26	100	3	30	---	9*
Air	CORONA DISCHARGE VIA TELSA COIL				---	7
	NON-FIBERIZED CONTROL				4000	16
	NON-FIBERIZED CONTROL				5540*	12*

TABLE 10

SHEAR STRENGTH AND PEEL STRENGTH FOR HEAVILY FIBERIZED
COUPONS BONDED WITH FM-73 ADHESIVE SYSTEM

GAS	FLOW RATE (cm ³ /min)	POWER (watts)	PRESSURE (torr)	TIME (min)	LAP SHEAR STRENGTH (lbs/in ²)	T-Peel STRENGTH (lbs/in.w)
---	---	---	---	---	1826*	3*
He	.95	100	.8	30	2990*	12*
O ₂	17	100	1.0	35	5500*	10*
O ₂	21	100	1	.04	1550*	10*
C ₂ H ₄	.2	4	.4	5	---	4*
Air	CORONA DISCHARGE VIA TELSA COIL				---	5
	NON-FIBERIZED CONTROL				4000	16
	NON-FIBERIZED CONTROL				5540*	12*

*Indicates adhesive used without mat carrier.

TABLE 11
SHEAR STRENGTH AND PEEL STRENGTH FOR COUPONS
BONDED WITH EPON 828 ADHESIVE SYSTEM*

SAMPLE	GAS	FLOW RATE (cm ³ /min)	POWER (watts)	PRESSURE (torr)	TIME (min)	LAP SHEAR STRENGTH (lbs/in ²)	T-PEEL STRENGTH (lbs/in.w)
Non-Fiberized Control	---	---	---	--	---	942	2.3
Heavily Fiberized	---	---	---	---	---	610	1.5
Heavily Fiberized	He	.95	100	---	30	740	---
Heavily Fiberized	O ₂	21	100	1.0	.04	730	**
Lightly Fiberized	---	---	---	---	---	1070	.9
Lightly Fiberized	He	.95	100	.1	30	---	1.9

* 12 mil glass beads were used to control bondline thickness.

**Not measurable.

polypropylene is activated by plasma exposure. Figure 47 and 48 show two sections of a heavily fiberized T-peel specimen bonded with the Epon 828 adhesive system. Characteristic fracture of these specimens resulted in three pieces created by two fracture planes running close to the anodic surface of each aluminum strip. Figure 47 shows a representative surface remaining on the aluminum coupon. This can be compared to the surface produced by the failure of an anodized non-fiberized control shown in Figure 49. The texture is somewhat different and it is suspected that the surface shown in Figure 47 is polypropylene, not adhesive. Figure 48 shows the surface of the adhesive layer fracture specimen. Here, fibers are clearly visible along with globular structures strikingly similar to those seen in Figure 47. It appears unlikely that these globules are adhesive which has permeated the dense fiber mat, therefore they are probably polypropylene. It is initially confusing to think that a fibrous mat could form above a film surface as indicated by these micrographs, but it could very well be that fiber agglomeration, trapped solution, and improper washing produced the underlying film. It can be concluded then, that in this case the film formation produced a weak link, but adhesive wetting or permeation was also a problem.

Another example of the adhesive wetting problem is shown clearly in Figures 50 and 51 which also depict two fracture pieces of a T-peel specimen bonded with the Epon 828 adhesive system. Figure 50 shows the aluminum coupon surface and an unwetted fiber mat can be clearly seen. Figure 51 shows the adhesive layer which also contains some of the in situ fiber mat. It is interesting to compare the fiber structures in Figures 50 and 51 with that in Figure 48. In the latter, the mat appears regular and quite similar in appearance to mats on unbonded coupons. In the other micrographs, the fibers appear to have been stretched and then allowed to snap back and this is most likely what has happened. The bulk of the fracture energy was then absorbed by the cleavage of the fiber mat in the case of the sample shown in Figures 50 and 51, and by the separation of a fiber mat from a film surface for the specimen shown in Figures 47 and 48. Another example of adhesive penetration difficulties is shown in Figure 52 which displays the surface of a fractured T-peel specimen

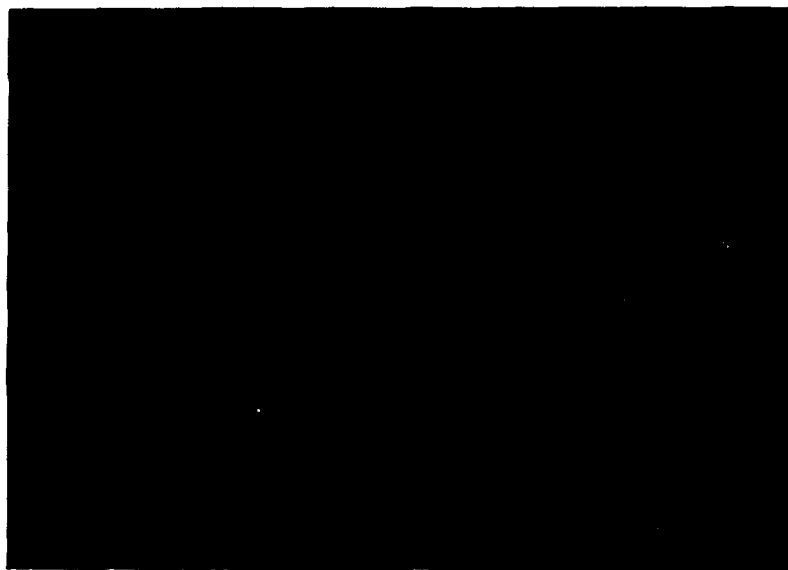


Figure 46. SEM Micrograph of Lightly Fiberized Unbonded Specimen. Magnification - 10,000X.



Figure 47. SEM Micrograph of a Fracture Surface of a Heavily Fiberized Coupon Bonded with Epon 828. Magnification - 9,000X.

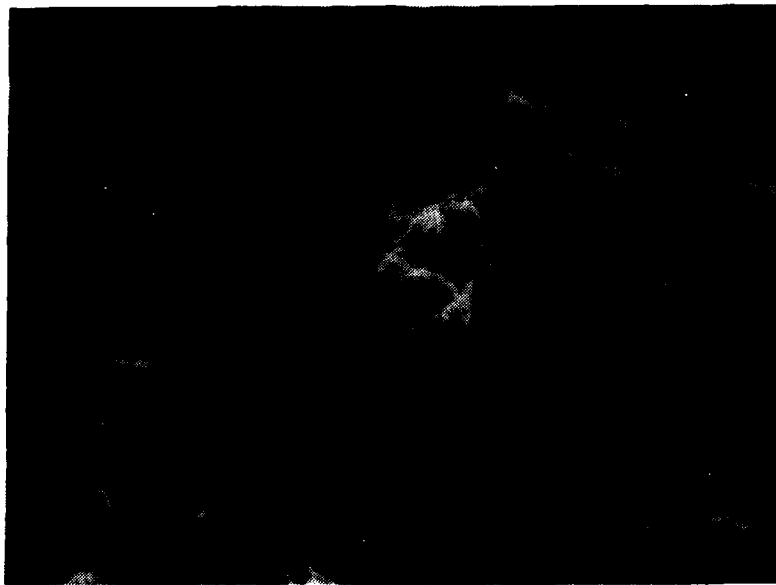


Figure 48. SEM Micrograph of Adhesive Layer Fracture Specimen. Magnification - 5,000X.



Figure 49. SEM Micrograph of Epon 828 Control Fracture Surface. Magnification - 14,000X.

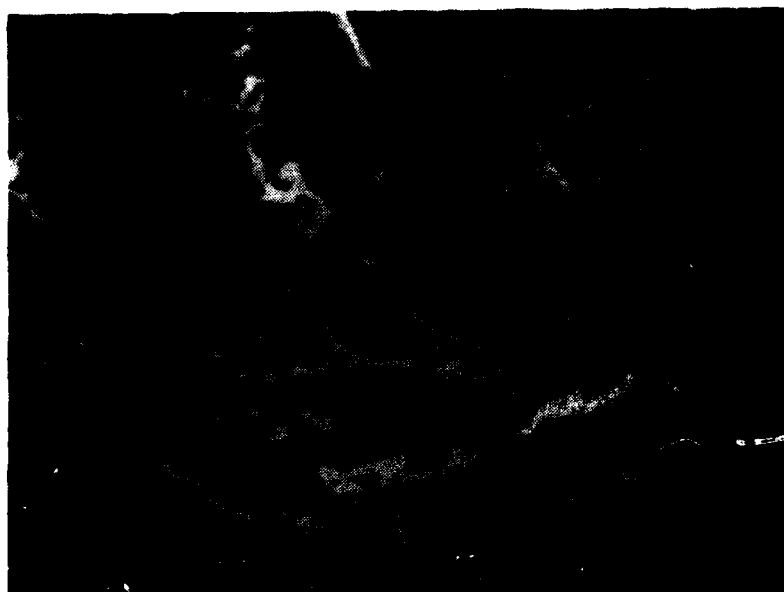


Figure 50. SEM Micrograph of Aluminum Coupon Fracture Surface of Lightly Fiberized Specimen. Magnification - 8,200X.

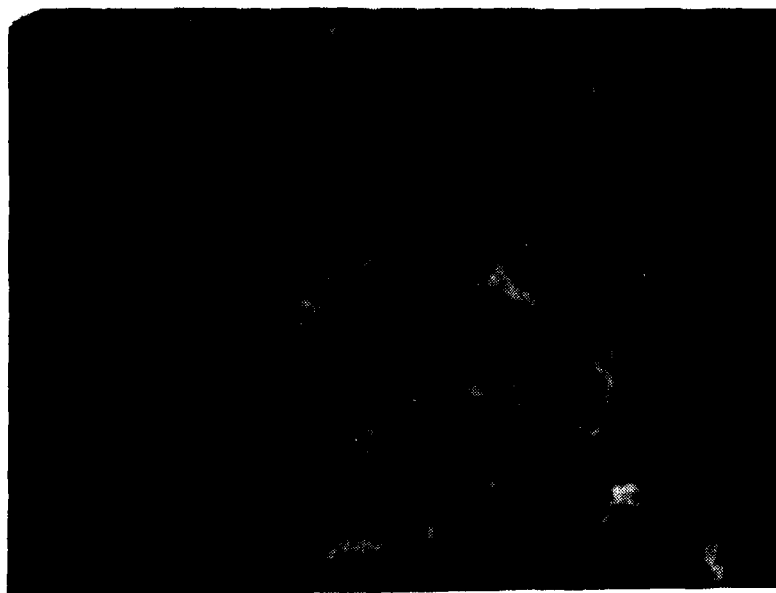


Figure 51. SEM Micrograph of Adhesive Film Fracture Surface of Lightly Fiberized Specimen. Magnification - 8,200X.

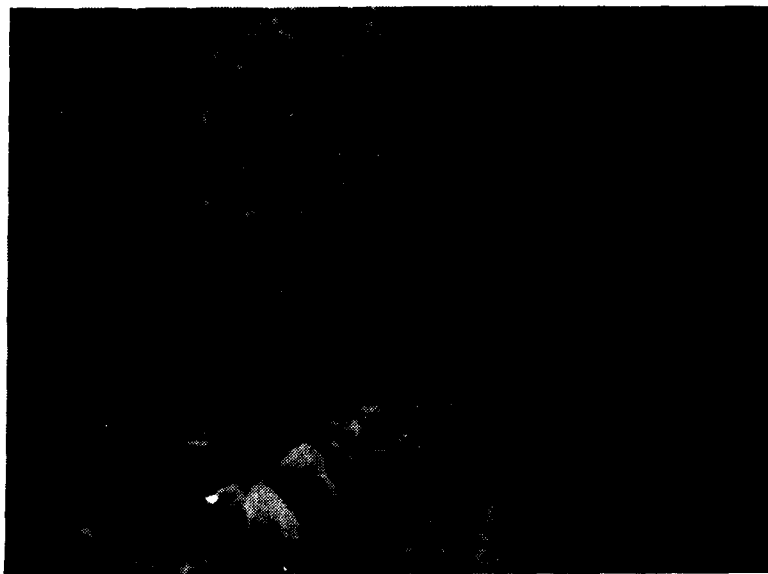


Figure 52. SEM Micrograph of Fiberized Specimen Bonded With FM-73. Magnification - 2,200X.

bonded with FM-73. The right hand portion of the micrograph is adhesive showing a fracture pattern typical for the material. In actuality, this picture was taken of mat containing adhesive and the adhesive surface observed has pulled away from the mat carrier. The left hand portion of the photograph appears to contain two types of fibers. The first type is the network fibers typically seen in SEM examination of fiberized, unbonded coupons. The second type, seen in the top of the micrograph, looks like the recoiled fibers discussed above. This photomicrograph indicates some penetration problems, but also shows that interaction and wetting are taking place. It is interesting now to look at Figures 53 and 54 which show another section of the sample.



Figure 53. SEM Micrograph of Fiberized Specimen Bonded With FM-73. Magnification - 1,600X.

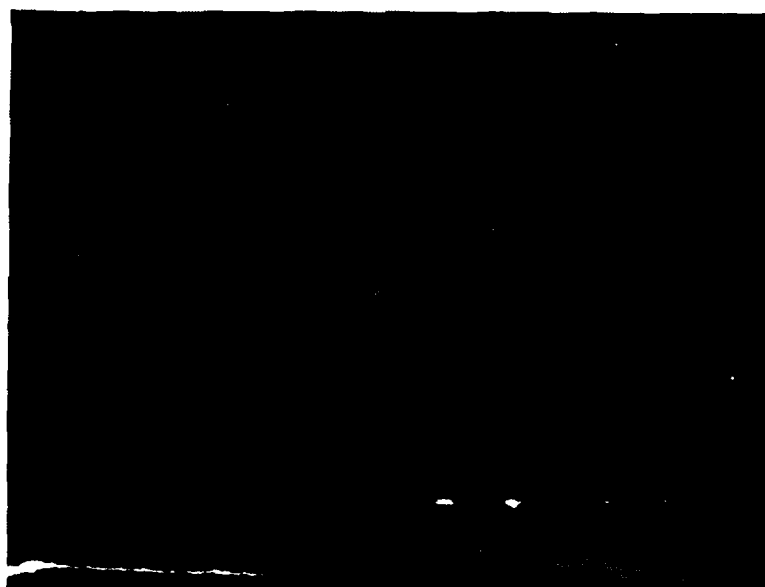


Figure 54. SEM Micrograph of Sample Shown Above at 16,000X magnification.

The adhesive appears to have failed in a more ductile mode and Figure 54 definitely indicates that fibers are being pulled along with the adhesive. The micrograph was taken very close to the anodic surface and the fibers in view have diameters in the range of what would be expected of ISF polypropylene material. One final piece of evidence to support this view is shown in Figure 55. This figure shows a SEM photo of FM-73 resin provided by the adhesive manufacturer. There was some original speculation that the fibers could be elongated regions of the dispersed nitrile rubber phase. However, after closer examination and outside consultation which shows these rubber particles remain spherical even after cleavage⁴⁵, this does not appear to be the case and the fibers are indeed ISF material.

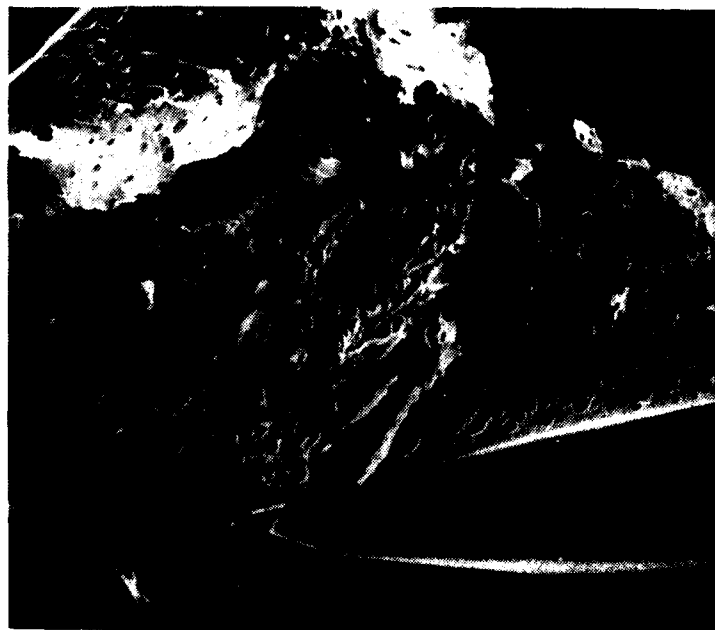


Figure 55. SEM Micrograph of FM-73 Adhesive.
Magnification - 2,200X.

Additional experimentation was undertaken to improve adhesive wetting by applying the FM-73 adhesive as a solution using methyl ethyl ketone as the solvent. Solutions of 5, 10, 20 and 40 percent solids were used. SEM micrographs still showed regions of sample which are without adhesive, indicating very little improvement was achieved. A minimum amount of mechanical property data was collected and it was similar to that listed in Tables 9 and 10. In summary, the failure analysis investigations did show that some in situ fiber adhesive interaction was occurring but that in many instances, either due to film formation or poor adhesive penetration, this effective interaction was probably the exception rather than the rule. This could very well explain why the mechanical property results were not more promising.

SECTION IV

CONCLUSIONS AND RECOMMENDATIONS

The intent of the program was to investigate the utility of in situ formed polypropylene fibers as a reinforcement to increase the peel and cleavage performance of adhesively bonded joints. Specifically, phosphoric acid anodized aluminum substrates were used with the aim of producing fibers directly in the pore structure which would extend out into and reinforce the adhesive resin.

Experimental results have shown that the in situ fibers formed do have dimensions compatible with the pore sizes of the anodic layers produced and there is some evidence to suggest that formation does take place within the pores. It was demonstrated that adhesion to the polypropylene material could be enhanced by plasma treatments; in particular, short time, medium power, oxygen exposures. Bonded T-peel and lap shear specimens were tested and the most promising results for fiberized specimens were in general equal to those obtained with non-fiberized control samples. Subsequent failure analysis revealed that problems of adhesive penetration and fiber film formation were responsible, at least in part, for the reduced mechanical performance.

Several issues raised during this program remain unanswered and are deserving of further investigation. The first is the formation of the desired fibers in the pore structure. It was demonstrated that an open pore structure seemed to be more conducive for fiber formation. This was further reinforced by the cursory examination of the fiberization potential of the proprietary etched samples. However, no definitive information was collected to ascertain fiber crystallization in the pores. Exploration of the silane attraction and nucleation concepts to promote in pore fiber formation proved interesting but was beset by complexities not soluble in this program. Additional ideas concerned with the directing of the solution flow field over the samples to produce strong extensional flow components were proposed but never attempted. It is clear that several directions exist in which to proceed further but any effort in this area must be coupled with a definitive analytical technique to monitor growth in the pore structure.

A second area of concern, which was not specifically discussed in detail in the text, was the uniformity of fiberization. It was very difficult to reproduce fiber formation from experiment to experiment and the uniformity of individual sample fiberization was also frequently not as good as desired. In addition, the structure of the in situ fiber mat must be controlled more effectively to reduce fiber agglomeration and allow adhesive penetration. Some progress has been made in this area on other programs³³, but considerable effort is still required.

Finally, the interaction of the in situ fibers and the adhesives requires further attention. It was assumed that the impenetrability of the fiber mats was the predominant cause of insufficient wetting. It could be that the plasma treatments used were not as effective as initially indicated. Also, even if fiber-adhesive interaction is maximized, it is not clear without further experiments whether true matrix reinforcement would occur.

In conclusion, this program has explored a truly interesting concept which may indeed have potential. The results obtained have served to show feasibility but considerably more developmental effort is required to demonstrate reduction to practicality.

REFERENCES

1. E. W. Thrall, *Adhesive Age*, 22 (10), 22 (1979).
2. AFFDL-TR-77-107, Final Report, "Primary Adhesively Bonded Structure Technology (PABST) General Material Property Data", Douglas Aircraft Company, September (1978).
3. W. George and P. Tucker, *Polym. Eng. and Sci.*, 15, 451 (1975).
4. J. Brandrup and E. H. Immergut, editors, *Polymer Handbook*, pg. IV-4, John Wiley and Sons, New York (1975).
5. A. Peterlin, *Polym. Eng. Sci.*, 16 (3), 126 (1976).
6. "Flow Induced Crystallization", R. H. Miller, ed., Gordon and Breach, New York (1979).
7. A. J. Pennings and A. M. Kiel, *Kolloid Z and Z Polymere*, 205, 160 (1965).
8. A. J. Pennings, R. Lageveen, and R. S. deVries, *Colloid and Polym. Sci.*, 255, 532 (1977).
9. A. Keller and F. M. Willmouth, *J. Macromol. Sci. - Phys.*, B6(3), 493 (1972).
10. A. J. Pennings, J. M. A. A. vanderMark, and A. M. Kiel, *Kolloid Z and Z Polymere*, 237, 336 (1970).
11. A. J. McHugh and E. H. Forrest, *J. Polym. Sci. - Physics*, 13, 1643 (1972).
12. A. G. Wikjord and R. St. John Manley, *J. Macromol. Sci. - Physics*, B2(3), 501 (1968).
13. A. J. Pennings and A. Zwijnenburg, *J. Polym. Sci. - Physics*, 17, 1101 (1979).
14. J. Smook, J. C. Torfs, P. F. vanHutten and A. J. Pennings, *Polymer Bulletin*, 2, 293 (1980).
15. A. J. Pennings, J. M. A. A. vanderMark, and H. C. Booij, *Kolloid Z and Z Polymere*, 236, (1980).
16. M. R. Mackley, F. C. Frank and A. Keller, *J. Mat. Sci.*, 10, 1501 (1975).
17. M. R. Mackley and A. Keller, *Phil. Trans., R. Soc. London*, A(278), 29 (1975).
18. S. Torza, *J. Polym. Sci. - Physics*, 13, 43 (1975).

19. A. J. McHugh and J. M. Schultz, *Kolloid Z and Z Polymere*, 251, 13 (1973).
20. L. B. Keller and R. K. Jenkins, U.S. Patent No. 4,037,010.
21. L. B. Keller and R. K. Jenkins, *Nature*, 278, 439 (1979).
22. R. E. Kelchner, USAF Technical Report, AFWAL-TR-78-95, June 1978.
23. C. H. Sherwood and R. E. Kelchner, USAF Technical Report, AFWAL-TR-81-4051, July 1981.
24. M. R. Mackley, *Colloid and Polym. Sci.*, 253, 261 (1975).
25. A. J. McHugh and E. H. Forrest, *J. Macromol. Sci. - Phys.*, B11 (2), 219 (1975).
26. A. J. McHugh and C. Silebi, *Polym. Eng. and Sci.*, 16 (3), 158 (1976).
27. R. B. Williamson and W. F. Busse, *J. Appl. Phys.*, 38, 4187 (1967).
28. AFML-TR-76-118, Final Report, "Characterization of Surfaces Prior to Adhesive Bonding", Northrop Corporation, July (1976).
29. AFML-TR-79-4081, Final Report, "Environmental Durability of the Weldbond, FPL, and PABST Joining Systems", Northrop Corporation, July (1979).
30. SC5180.17FTR, Final Report, "Surface Treatment for Aluminum Bonding", Rockwell International Science Center, October (1979).
31. M. H. Stone and T. Peet, Royal Aircraft Establishment, Farnborough, Hants, U.K., Report RAE TM Mat 349, July 1980.
32. E. E. Peterson and D. B. Arnold, USAF Technical Report, AFWAL-TR-80-4176, March 1981.
33. C. H. Sherwood, U.S. Army Natick Laboratories, Contract No. DAAK60-81-C-0006, Final Report, February 1982.
34. C. H. Sherwood, unpublished work, Hughes Aircraft Company, 1981.
35. J. R. Hall, C. A. L. Westerdahl, A. T. Devine, and M. J. Bodnar, *J. Appl. Polym. Sci.*, 13, 2085 (1969).
36. Shonhorn and Hansen, *J. Appl. Polym. Sci.*, 11, 1461 (1967).
37. P. Blais, D. J. Carlsson, and D. M. Wiles, *J. Appl. Polym. Sci.*, 15, 129 (1971).
38. H. Schonhorn and R. H. Hansen, *J. Appl. Polym. Sci.*, 11, 1461 (1967).

39. H. Schonhorn, F. W. Ryan and R. H. Hansen, *J. Adhesion*, 2, 93, (1970).
40. J. R. Hollahan and A. T. Bell, editors, Techniques and Applications of Plasma Chemistry, Ch. 3, John Wiley and Sons, New York (1974).
41. H. Schonhorn and F. W. Ryan, *Adv. Chem. Ser.*, 87, 140 (1968).
42. L. Pospisil, J. Janca and L. Ambroz, *Folia Fac. Sci. Nat. Univ. Purkyhianae Brun.* 18(3), 67 (1977).
43. R. H. Hansen, J. V. Pascale, T. DeBenedictis and P. M. Rentzepis, *J. Polym. Sci.*, 3, 2205 (1965).
44. A. Moshonov and Y. Avny, *J. Appl. Polym. Sci.*, 25, 771 (1980).
45. Private Communication, James Noland, American Cyanamid Company, Stamford, Conn., April, 1982.

2-8

DT